Journal of Medicinal Chemistry

Article

Design, Synthesis and Preclinical Evaluation of 3-Methyl-6-(5-thiophenyl)-1,3-dihydro-imidazo[4,5-*b*]pyridin-2-ones as Selective GluN2B Negative Allosteric Modulators for the Treatment of Mood Disorders

Christa C Chrovian, Akinola Soyode-Johnson, Brice Stenne, Daniel J. Pippel, Jeffrey Schoellerman, Brian Lord, Alexandra S Needham, Chunfang Xia, Kevin J Coe, Kia Sepassi, Freddy Schoetens, Brian Scott, Leslie Nguyen, Xiaohui Jiang, Tatiana Koudriakova, Bartosz Balana, and Michael A Letavic

J. Med. Chem., **Just Accepted Manuscript** • DOI: 10.1021/acs.jmedchem.9b02113 • Publication Date (Web): 31 Jul 2020

is published by the American Chemical Society. 1155 Sixteenth Street N.W., Washington, DC 20036

Design, Synthesis and Preclinical Evaluation of 3-Methyl-6-(5-thiophenyl)-1,3-dihydro-imidazo[4,5-*b*]pyridin-2-ones as Selective GluN2B Negative Allosteric Modulators for the Treatment of Mood Disorders

AUTHOR NAMES. Christa C. Chrovian, Akinola Soyode-Johnson, Brice Stenne, Daniel J. Pippel, Jeffrey Schoellerman, Brian Lord, Alexandra S. Needham, Chungfang Xia, Kevin J. Coe, Kia Sepassi, Freddy Schoetens, Brian Scott, Leslie Nguyen, Xiaohui Jiang, Tatiana Koudriakova, Bartosz Balana, and Michael A. Letavic.*

AUTHOR ADDRESS Janssen Research & Development, LLC, 3210 Merryfield Row, San Diego, California 92121-1126, United States.

KEYWORDS. NMDA, NR2B, antagonist, enabling formulation, receptor occupancy, autoradiography, biodistribution, non-clinical studies, toxicokinetics, GluN2B NAM.

ABSTRACT. Selective inhibitors of the GluN2B subunit of *N*-methyl-*D*-aspartate receptors in the ionotropic glutamate receptor superfamily have been targeted for the treatment of mood disorders. We sought to identify structurally novel, brain penetrant, GluN2B-selective inhibitors suitable for evaluation in a clinical setting in patients with major depressive disorder. We identified a new class of negative allosteric modulators of GluN2B that contain a 1,3-dihydro-imidazo[4,5-*b*]pyridin-2-one core. This series of compounds had poor solubility properties and poor permeability, which was addressed utilizing two approaches. First, a series of structural modifications was conducted which included replacing hydrogen bond donor groups. Second, enabling formulation development was undertaken in which a stable nanosuspension was identified for lead compound **12**. Compound **12** was found to have robust target engagement in rat with an ED_{70} of 1.4 mg/kg. The nanosuspension enabled sufficient margins in pre-clinical

toleration studies to nominate **12** for progression into advanced good laboratory practice studies.

INTRODUCTION. The neurotransmitter glutamate is prevalent to such an extent in the central nervous system (CNS) of complex organisms that it is involved in nearly all aspects of normal CNS functioning and it is used by most excitatory synaptic connections in the mammalian brain. Glutamate regulates the activity of two classes, or superfamilies, of receptors: metabotropic glutamate receptors that are G protein-coupled receptors (GPCRs) and ionotropic glutamate receptors (iGluRs) that are ion channels. Ionotropic glutamate receptors function as tetramers and each contain two clamshell-shaped extracellular N-terminal domains, a ligand binding domain, a transmembrane domain and an intracellular C-terminal domain.[1] The most well studied iGluRs are the α-amino-3-hydroxy-5-methyl-4-isoxazolepropionic acid (AMPA) and *N*-methyl-*D*-aspartate (NMDA) receptors. A key distinction between the two classes is that AMPA receptors are active during basal synaptic transmission whereas NMDA receptors are activated only after a depolarization event of the surrounding neuronal membrane, because Mg^{2+} blocks the

pore under basal conditions. When the Mg^{2+} block is relieved after a depolarization event, the pore becomes permeable to Ca^{2+}. The influx of Ca^{2+} through NMDA receptors triggers signaling cascades and regulates gene expression that is critical for different forms of synaptic plasticity, including both long-term potentiation (LTP)[2] and long-term depression (LTD).[3] Growing evidence suggests that disturbances in brain and synaptic plasticity mediated by the glutamate system contribute to the pathophysiology of mood disorders.[4-6]

The NMDA receptor tetramers are comprised of two GluN1 and two GluN2 subunits. Four unique GluN2 subunits have been identified and they have been assigned the nomenclature GluN2A-GluN2D. The receptors require co-activation by both glycine (D-serine) and glutamate, which bind to GluN1 and GluN2, respectively.[1,7]

The four GluN2 subunits of the NMDARs exhibit distinct distribution patterns across the mammalian brain, depending on the species and individual's development age. For adult mammals, GluN2B subunits are expressed primarily in the cortex, striatum, and notably the hippocampus, a region consistently demonstrating the highest receptor density throughout the full life cycle.[8-9]

The NMDA receptor has been studied extensively since the early 1980s when it was determined that Mg^{2+} confers a blockade of the ion channel under basal conditions, which is the salient feature conferring its voltage dependence.[10-11] Selectively blocking the function of GluN2B-containing receptors, on the other hand, was targeted later, when it was determined that ifenprodil (**1**) discriminates the subtypes of NMDAR.[12] Compound **1** is an anti-hypertensive agent discovered in the 1960s that is a highly potent inhibitor of the GluN2B subunit, in addition to being a significant modulator of alpha adrenergic and sigma receptors.[13]

Compound **1** is a negative allosteric modulator (NAM) that was found to bind to the NMDAR complex at a site positioned between the GluN1 and GluN2B subunits.[14] The site is not present on the other three GluN2 subunits and inhibitors binding at this interface have excellent selectivity for GluN2B over GluN2A, GluN2C and GluN2D. This feature has enabled the scientific community the opportunity to evaluate the safety and pharmacology of several NMDAR small molecule modulators that are exquisitely selective for GluN2B versus the other three GluN2 subunits.[15-17] Several NAMs have

been evaluated in clinical settings, two of which were assessed in patients with depressive disorders.

The first reported GluN2B-selective NMDAR inhibitor assessed in patients diagnosed with major depressive disorder was CP-101,606 (**2**, traxoprodil).[17] Compound **2** was originally discovered by Pfizer through a medicinal chemistry program based on **1**. It was identified as an inhibitor of NMDA receptor function and was shown to be neuroprotective in vitro against glutamate toxicity.[18] As the tetrameric structure of the NMDA receptor was unknown at the time, the selectivity of **2** for the GluN2B subunit was not revealed until later.[19] Compound **2** progressed into clinical trials in subjects with traumatic brain injury.[20] Several years later it was assessed in patients diagnosed with treatment resistant depression (TRD) in Phase II clinical trials as an add on therapy to paroxetine. It achieved a positive response in 60% of subjects in a current depressive episode.[17] Compound **2** has limited oral bioavailability and its route of administration was intravenous (i.v.). The cardiovascular safety of **2** was also limited due to observed QT interval prolongation, and trials were ceased.

CERC-301 (**3**, Rislenemdaz, MK-0657) is an orally available GluN2B-selective NAM discovered by Merck, and was originally intended for Parkinson's disease or pain and related disorders.[21-23] The results of a Phase II study were reported in 2009 in which **3** did not result in motor function improvement in patients with Parkinson's disease.[22] It was later developed for the treatment of major depressive disorder (MDD) and evaluated in two Phase II trials in patients with MDD.[23-26] The drug was generally well tolerated and there were no discontinuations due to adverse events (AE). Both trials failed to meet their Primary Endpoints, although in the second of the two Phase II studies, a notable improvement in symptoms was measured on Day 2 as determined by the secondary rating scale called the Hamilton Depression Rating Scale (HDRS-17).[25,26]

The goal of medicinal chemistry efforts in our drug discovery program was to identify novel GluN2B-selective NAMs that were well tolerated and suitable for once a day oral dosing in the clinic, in order to assess their performance in patients with psychiatric (mood) disorders.

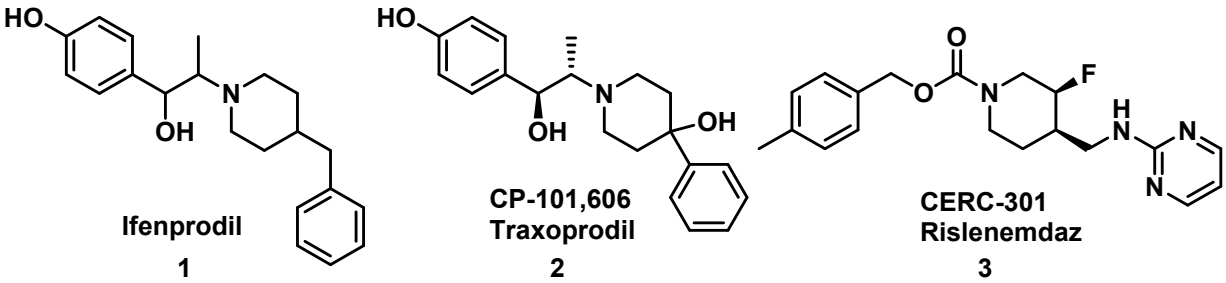

Figure 1. GluN2B selective negative allosteric modulators.

RESULTS AND DISCUSSION:

A high-throughput screening (HTS) campaign identified compounds that inhibited functional activity of human GluN1a/GluN2B channels expressed in CHO cells as measured by Ca^{2+} flux (FLIPR) elicited by addition of co-agonists glutamate and glycine. Confirmed hits were counter-screened in heterologous cells expressing human GluN1a/GluN2A. From this effort, a selective series of GluN2B inhibitors containing a 1,3-dihydro-imidazo[4,5-*b*]pyridin-2-one core was identified. Compound **4** was potent in the FLIPR assay (hGluN2B IC_{50} = 22 nM) and was selective over the GluN2A, GluN2C, GluN2D subunits (IC_{50}s all > 10 μM). Two salient features of **4**, however, were its poor solubility (<4 μM at pHs 2 and 7) and high efflux ratio (B-A/A-B =18). Compound **4** has two hydrogen bond donors and a characteristically insoluble urea moiety[27] imbedded in

the core, likely contributing to its P-glycoprotein (Pgp) substrate potential, indicated by its high efflux ratio in the MDCK cell line transfected with MDR1. Compounds with efflux ratios >10 are expected substrates for Pgp and are less likely to cross the blood brain barrier (BBB) and access the brain compartment. We were therefore encouraged to find that eliminating the H-bond donors by replacing the cyclopropyl- of the secondary amide with azetidine to provide instead a tertiary amide, and adding *N*-methyl substitution at the urea *N*-H, resulted in compounds such as **5** that have comparable GluN2B potency to **4**. Compound **5** had a GluN2B IC_{50} of 112 nM and measurable solubility (23 μM at pH 7). Compound **5** also had an improved efflux ratio (9.3) and a higher plasma free fraction (5.2%) than **4** (0.4%). Neither **4** nor **5** displayed hERG channel inhibition. The majority of subsequent 1,3-dihydro-imidazo[4,5-*b*]pyridin-2-one core compounds that were synthesized and assessed for hERG inhibition, including all of those described in this manuscript, also had hERG IC_{50} values >10 μM.

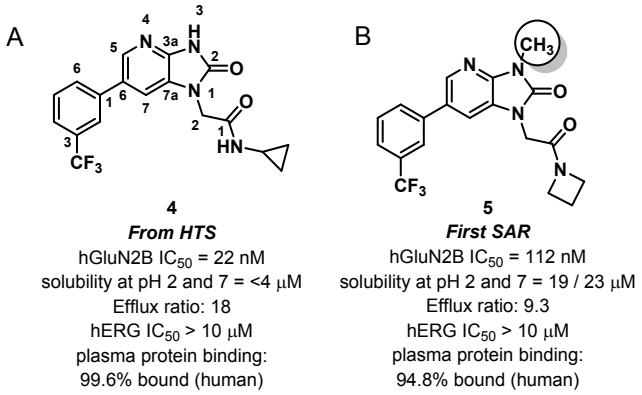

Figure 2. GluN2B selective negative allosteric modulators. (A) Compound **4** was identified from a high throughput screen. (B) Compound **5** shows improved aqueous solubility, efflux ratio and human plasma protein binding compared to HTS hit **4**.

The early SAR of the 1,3-dihydro-imidazo[4,5-*b*]pyridin-2-one series indicated that poor solubility was one of the prominent features of the core, which was predicted to be an obstacle. However, low metabolic turnover in vitro was also observed, a feature that was preferred. One trend that we focused on for optimization was the high efflux ratios that appeared to be the result of Pgp-mediated efflux. It was rationalized that if drug candidates could be identified that have both high intrinsic permeability and relatively low efflux liability, the need for high thermodynamic solubilities could be somewhat obviated.[28] Our strategy for the 1,3-dihydro-imidazo[4,5-*b*]pyridin-2-ones was to negotiate solubility

properties in such a way that suitable absorption, distribution, metabolism and excretion (ADME) in this series could be achieved, as well as good GluN2B potencies and brain uptake. Since much of the early SAR on the 1*H*-pyrrolo[3,2-*b*]pyridines has already been disclosed,[29] a deeper focus of this disclosure will be Late Lead Optimization SAR, in vivo data and formulations that enabled clinical candidate selection.

The first 1,3-dihydro-imidazo[4,5-*b*]pyridin-2-one compounds prepared had a *meta*-trifluoromethylphenyl group at the 6-position of the 1,3-dihydro-imidazo[4,5-*b*]pyridin-2-one core (referred to as left hand side (LHS) throughout this discussion, Table 1: **5**-**7**). These analogs had moderate human GluN2B potencies (IC_{50} values of 47-118 nM) and their efflux ratios were moderately high, ranging from 7-9 (Table 1). In the presence of a Pgp inhibitor, their permeability was very good, ranging from P_{app} = 35 to 68 (x 10^{-6} cm/sec), suggesting that the measured cellular efflux potential is Pgp mediated. *N*-Azetidine containing amides **5** and **7** had comparable solubilities in aqueous buffer, although *N,N*-dimethylamide **6** had measurably less (6 μM at pH 2 and 7).

Table 1. GluN2B potency and affinity and in vitro ADME for 3-methyl-6-(3-(trifluoromethyl)phenyl)-1,3-dihydro-imidazo[4,5-*b*]pyridin-2-ones.

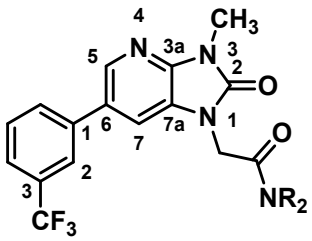

cpd	NR_2	GluN2B IC_{50}[a] (nM)	GluN2B K_i[b] (nM)	Solub at pH 2/7[c]	ER (hu/r)[d]	Efflux ratio[e]	P_{app}[f]
5		97, n=1	19 ± 7	19 / 23	<0.3 / <0.2	9.0	39
6		47, n=1	19, n=1	6 / 6	0.38 / 0.31	7.0	35
7	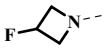	118 ± 82	25 ± 21	17 / 16	<0.3 / <0.2	7.0	68

[a] IC_{50} values were determined by a calcium mobilization assay in inducible CHO T-Rex cells heterologously expressing the hGluN1a/GluN2B receptor. Values reported are the mean ± SD of at least three experiments unless otherwise stated. [b] K_i values were determined using a radioligand competitive binding assay in rat cortex membranes using 3-[^{3}H] 1-(azetidin-1-yl)-2-[6-(4-fluoro-3-methyl-phenyl)pyrrolo[3,2-*b*]pyridin-1-yl]ethanone.[29] Values reported are the mean ± SD of at least three experiments unless otherwise stated. [c] Kinetic solubility in aqueous buffer. [d] Stability in human and rat liver microsomes. Data reported as microsomal extraction ratio. [e] Efflux ratio was measured

using MDCK-MDR1 cells transfected with the P-glycoprotein (MDR-1). The efflux ratio is reported as the ratio of velocities (B-A/A-B). [f] Papp is A to B permeability (10^{-6} cm/s) measured in the presence of 2 μM of the PgP inhibitor elacridar.

A strategy to lower efflux ratios emerged at around this point in the SAR, when concurrent work on a second series of GluN2B NAMs containing a 1*H*-pyrrolo[3,2-b]pyridine core indicated that somewhat lower efflux ratios were measured for many of the examples had thiophenes on the LHS as phenyl bioisosteres.[29] An example from that report in which 4-fluoro-3-methylphenyl was applied to the 1*H*-pyrrolo[3,2-b]pyridine core LHS (**8**, Figure 3) had an efflux ratio of 5.4 and plasma C_{max} of 1380 ng/mL in rat, whereas the comparator molecule with a 5-(trifluoromethyl)thiophen-2-yl group in place of 4-fluoro-3-methylphenyl (**9**), had an efflux ratio of 3.5 and higher C_{max} of 2330 ng/mL in rat (Figure 3).[29] We were thus prompted to apply these learnings and revisit thiophenes with the 1,3-dihydro-imidazo[4,5-*b*]pyridine-one core, hopeful that the combination of high plasma exposure and low efflux ratios in the pyrrolo[3,2-b]pyridine series would translate to the 1,3-dihydro-imidazo[4,5-*b*]pyridine-one core, and also lead to pharmacologically relevant brain exposures.

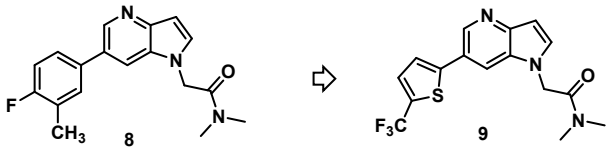

hGluN2B IC_{50} = 25 nM
Solubility at pH 2 and 7 = >400 / 264 μM
Efflux ratio: 5.4
in vivo PK rat 5 mg/kg p.o.
AUC: 1587 h*ng/mL
C_{max}: 1380 ng/mL

hGluN2B IC_{50} = 47 nM
Solubility at pH 2 and 7 = >400 / 100 μM
Efflux ratio: 3.5
in vivo PK rat 5 mg/kg p.o.
AUC: 4728 h*ng/mL
C_{max}: 2330 ng/mL

Figure 3. Summary of 1H-pyrrolo[3,2-b]pyridine series SAR.[29]

The thiophene LHS SAR for the 1,3-dihydro-imidazo[4,5-*b*]pyridin-2-one core indicated that methyl- or fluoromethyl- groups incorporated at the 5-position (of thiophen-2-yl) were generally effective in both human GluN2B and rat GluN2B binding assays (Table 2). Analogs had poorer IC_{50} and K_i values when the ring substitution was at the 4-position of the thiophene compared to the 5-position (**10** vs **11**). Trifluoromethyl thiophene analogs with *N*,*N*-dimethylacetamid- or 2-(azetidin-1-yl)-2-oxoethyl groups were potent NAMs (**12**: IC_{50} = 31 nM, **13:** IC_{50} = 29 nM) with robust rat GluN2B K_i values (**12:** K_i = 16 nM, **13:** K_i = 12 nM). 5-Cyclopropyl substituted thiophenes were tolerated (**17**: IC_{50} = 81 nM, n=1) but were not as potent as the corresponding methyl (**11**: IC_{50} = 25 nM) or fluoromethyl (**12:** IC_{50} = 31 nM, **15:** IC_{50} = 6 nM) analogs.

The efflux ratios for methyl and trifluoromethyl-substituted thiophenes were in the desirable range of 1.4 to 3.7 (**10**-**14**) and lower than for compounds **5-7**, as we had hoped. Intrinsic permeability values (P_{app}) for **10**-**14** were excellent (37 to 68 x10^{-6} cm/sec). Given their low efflux ratios (<4) and high P_{app}, compounds **10**-**14** were predicted to be BBB penetrant. Difluoromethyl thiophenes **15** and **16** had higher efflux ratios (5.8 and 9.1, respectively) but they were found to decompose in aqueous buffer after 24 h at pHs 2 and 7. So despite its excellent potency, compound **15** (hGluN2B IC_{50} = 6 nM) was deprioritized due to its chemical instability.

The trifluoromethyl-substituted phenyl LHS (**5-7**) and thiophene LHS (**12**-**14**) showed excellent stability in human and rat liver microsomes. Extraction ratios (ER) were moderate for difluoromethyl-substituted thiophenes (**15**-**16**) and poor for 4- and 5-methyl-substituted thiophenes (**10**-**11**).

The solubility of compounds **5-7** was moderately low at both pHs 2 and 7. Examples that contained a trifluoromethylthiophene (**12**-**14**) displayed low solubility below the limit of the assay (<4 μM).

Table 2. GluN2B potency and affinity and in vitro ADME for 3-methyl-6-(thiophenyl)-1,3-dihydro-imidazo[4,5-*b*]pyridin-2-ones.

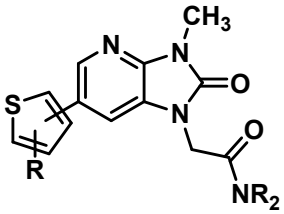

cpd	NR_2	Thio-phene	GluN2B IC_{50}[a] (nM)	GluN2B K_i[b] (nM)	Solub at pH 2/7[c]	ER (hu/r)[d]	Efflux ratio[e]	P_{app}[f]
10		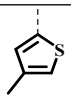	216 ± 85	270 ± 59	31 / 25	0.59 / 0.82	3.5	38
11			25 ± 7	44 ± 31	48 / 39	0.56 / 0.78	3.2	37
12		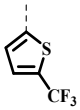	31 ± 16	16 ± 7	<4 / <4	<0.3/<0.17	2.1	47
13		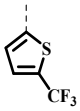	29 ± 9	12 ± 3	<4 / <4	<0.3 / <0.17	1.4	54

14	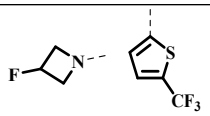	71 ± 30	21 ± 9	<4 / <4	<0.3/<0.17	3.7	68
15	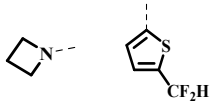	6 ± 5	19 ± 12	decomp	0.46/0.58	5.8	41
16	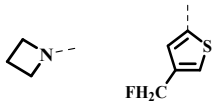	79 ± 63	59± 25	decomp	<0.3 / 0.52	9.1	51
17	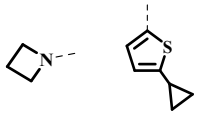	81, n=1	63, n=1	nd	nd	nd	nd

[a-f] Same as Table 1.

Ultimately, compounds **12**-**14** were prioritized over the other examples due to their low microsomal turnover and GluN2B activity, both in the human recombinant cell line and in rat cortex binding assay. It is of note, however, that **12**-**14** were the least soluble of the series and possible challenges were anticipated due to their poor solubility properties. Compounds **15**-**16** looked promising, but were not stable at pH 2 or 7 in aqueous buffer after 24 h. Compound **11** was soluble in buffer up to 39 and 48 μM at pHs 2 and 7, respectively, making it the most soluble of present examples. However, it had moderately

high turnover in liver microsomes, with a human ER of 0.56. If **11** were to exhibit a good correlation between in vitro and in vivo PK (IVIVC) in rat, this predicted ER value would not preclude a therapeutically relevant C_{max} and oral bioavailability in human. Although it was foreseeable that intestinal dissolution may not be a limiting factor in absorption of **12-14**, in which case plasma drug concentrations could still reach levels well in the range of many drug substances that demonstrate robust bioavailabilities, due to the uncertainty surrounding proper absorption of **12-14** into systemic circulation, **11** was also selected for in vivo progression.

The synthesis of **5-7** and **10-11** was conducted using a sequence beginning with 2-chloro-5-bromo-3-nitropyridine, which underwent an S_NAr reaction with aqueous methylamine at rt. The nitro group was reduced to the primary amine with zinc in the presence of ammonium chloride and the 1,3-dihydro-imidazo[4,5-*b*]pyridine-one core was formed in the next step using 1,1'-carbonyldiimidazole (CDI). Intermediate **18** was deprotonated with NaH and underwent S_N2 addition to ethyl 2-bromoacetate to give **19** in 88% yield. Lithium hydroxide was used to saponify ester **19** to carboxylic acid **20**, which was subjected to amide forming conditions using propanephosphonic acid anhydride

(T3P), followed by Suzuki coupling to provide final products **5-7** and **10-11**. For the formation of final products containing the 5-(trifluoromethyl)thiophen-2-yl moiety (**12-14**), ethyl ester **19** was subjected to Suzuki coupling conditions to first append the 5-(trifluoromethyl)thiophen-2-yl group to give **24**, and then ester hydrolysis and amide formation gave final products **12-14**. The synthesis of final products **15-17** was conducted through Suzuki couplings of **22** and thiophene boronic esters.

Scheme 1. The synthetic route for compounds **5-7** and **10-17**.[a]

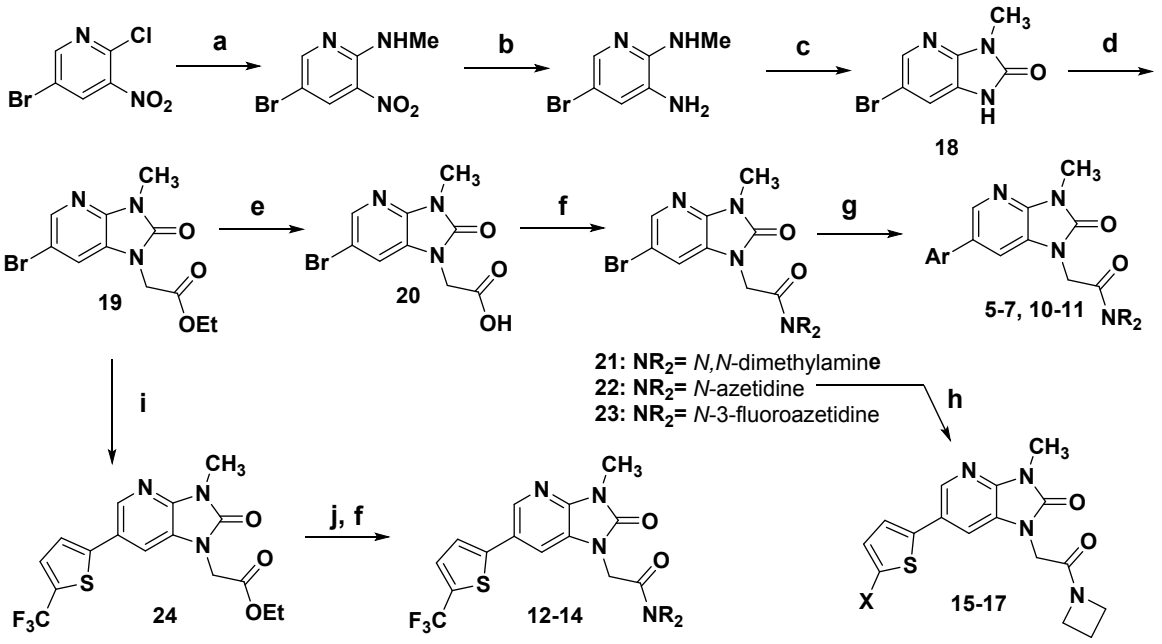

[a] Reagents and conditions: (a) 40% NH_2CH_3 in water, THF, 0 °C, then rt 16 h (99%); (b) zinc, ammonium chloride, acetone/water (10:1), rt, 72 h; (c) CDI, DMF, rt to 60 °C, 16 h (88% over 2 steps); (d) sodium hydride, DMF, rt, 30 min; then 2-bromoethylacetate, DMF,

rt, 4 h, 88%; (e) lithium hydroxide, THF/water, rt, 16 h (83%) (f) secondary amine, *n*-propylphosphonic anhydride (T3P®, 50% in ethyl acetate), Hunig's base, CH_2Cl_2, rt, 16 h (61-85%) (g) Boronic Acid, cesium carbonate, $PdCl_2$(dppf), dioxane, 100 °C, 16 h (9-46%) (h) Bromothiophene, bis(pinacolato)diboron, potassium acetate, $PdCl_2$(dppf), dioxane, 90 °C, 2 h; then add **22**, cesium carbonate, 90 °C, 3h addnl. (10-48%); (i) 4,4,5,5-tetramethyl-2-(5-(trifluoromethyl)thiophen-2-yl)-1,3,2-dioxaborolane, potassium carbonate, $PdCl_2$(dppf), toluene/water (10:1), 105 °C, 3 h (91%); (j) lithium hydroxide, THF/water, rt, 16 h (98%).

Compounds **12**-**14** were evaluated in PK experiments in rat followed by receptor occupancy studies in the rodent brain (Table 3). Compound **11** was evaluated in rat PK experiments as well but showed very high i.v. CL, suggestive of extra-hepatic clearance mechanisms, as well as low bioavailability (1%). As such, it was not further assessed in receptor occupancy studies. Compounds **12**, **13** and **14** all had low to moderate CL (14-30 mL/mg/kg) and moderate volumes of distribution (V_{ss}) (0.9-1.9 L/kg). All three compounds had excellent bioavailabilies, indicative of complete absorption. It is of note that **13** was found to be insoluble at 0.5 mg/mL in three standard excipients, 20% hydroxypropyl-β-cyclodextrin (HP-β-CD), 30% sulfobutylether-β-cyclodextrin (SBE-β-CD)

and 100% polyethylene glycol 400 (PEG-400). The 20% HP-β-CD formulation did allow for a 0.1 mg/mL solution, which was enough to support a 0.5 mg/kg dose study.

Next, GluN2B receptor occupancy and brain concentrations were measured for **12, 13** and **14** over a six-hour time course after oral administration in rat (Table 3). Receptor occupancy was assessed by autoradiography (ARG) by application of the GluN2B-selective ^{3}H radiotracer 3-[^{3}H] 1-(azetidin-1-yl)-2-[6-(4-fluoro-3-methyl-phenyl)pyrrolo[3,2-*b*]pyridin-1-yl]ethanone[29] to brain slices ex vivo. Thirty min after dosing at 3 mg/kg, all three compounds showed >70% occupancy as measured against background control. At 6 h, **13** had >70% GluN2B occupancy, although brain concentrations decreased from 1257 ng/mL at 2 h (Table 2) to 598 ng/g at 6 h (full data shown in SI). Due to the difficulty in formulating **13**, however, it was decided to deprioritize **13** and progress **12**.

Table 3. Pharmacokinetic data (0.5 mg/kg i.v / 2.5 mg/kg p.o., n=3 ± SD, vehicle: 20% HP-β-CD) and GluN2B occupancy (3 mg/kg p.o., n=2 ± SEM) data for **11-14** in rat.

	Cl (mL/mi	V_{ss} (L/kg)	$t_{1/2}$ (h)	C_{max} (ng/mL)	AUC_{inf} (hr·ng/	$t_{/max}$ (h)	%F	% Occupancy Timecourse (3 mg/kg	C_{max} -brain	T_{max} (h)

	n/kg)				mL)			p.o.)[a] (vehicle: 20% HP-β-CD)			g)	
								0.5 h	**2.0 h**	**6.0 h**		
11	114 ±24	1.1 ±0.3	0.2 ±0.0	6±3	--	--	1±1	--	--	--	--	--
12[b]	30±0.9	1.9 ±0.1	0.8 ±0.0	479 ±172	1829 ±535	1.3 ±0.6	132 ±39	87 ±2.3	76 ±1.6	31, n=1	765 ±91	0.5
13[c]	14±6	1.2 ±0.1	1.3 ±0.3	188 ±68	912 ±50	1.0 ±0.0	121 ±38	79 ±2.0	80 ±0.9	77 ±2.2	1257 ±128	2.0
14[d]	20±18	0.9 ±1	0.9 ±0.6	1001 ±235	3614 ±240	1.0 ±0.0	109 ±7	74 ±3.9	71 ±0.7	24 ±1.0	728 ±128	2.0

[a] Ex vivo GluN2B labelling was expressed as the percentage of GluN2B labelling in corresponding brain areas of vehicle-treated animals.[b] Vehicle is 1:1 PEG400/water for PK study. [c] Doses were 0.1 mg/kg iv and 0.5 mg/kg p.o. [d] Vehicle is 30% SBE-β-CD for PK study.

The brain biodistribution of **12** was evaluated in rodents in a microdosing experiment, in order to obtain a preliminary assessment of brain uptake of **12** in brain regions known to be enriched with the GluN2B subunit. Although NMDA-subunit expression has been shown to change in the mammalian brain from infancy to adulthood, the hippocampal region has the highest receptor density of GluN2B protein and mRNA throughout the lifetime. GluN2B is also highly expressed in the cortex, and moderately in the striatum. GluN2B is not expressed in the cerebellum.

Rats (n = 3 each group) were administered a single i.v. dose of 0.03 mg/kg of **12** formulated in 50% (w/v) PEG/water at pH 7.4. Animals were sacrificed at 5, 10, 30, 60- and 120-min following dosing. The cerebellum, cortex, striatum and hippocampus were collected. The sample weight was measured and then homogenized to analyze levels of **12** by LC-MS/MS.

Compound **12** was detected in all four brain regions at each timepoint (Figure 4). In the cerebellum, concentrations were highest at the 5 min timepoint (19.3 ± 1.08 ng/mL) and decreased over time to 6.9 ± 0.65 ng/mL at 120 min, consistent with null expression of GluN2B in rat cerebellum. In the cortex, concentrations of **12** were higher at 10 min compared to 5 min and decreased at each of the subsequent timepoints. The highest levels of **12** were measured at 10, 30 and 60 min in the hippocampus, where GluN2B is highly enriched. Levels in the hippocampus reached a significance versus the cerebellum at 30 min (22.7 ± 2.49 vs. 13.8 ± 1.62 ng/ mL in cerebellum, $P<0.05$) and 60 min (20.9 ± 3.47 vs.11.9 ± 1.27 ng/ mL in cerebellum, $P<0.05$) time points. At 120 min after dosing, both hippocampus and striatum showed higher levels of **12**, reaching significance (10.1±0.13 and 9.8±0.20 ng/ mL respectively) vs. cerebellum (6.9±0.65 ng/ mL) $P<0.05$.

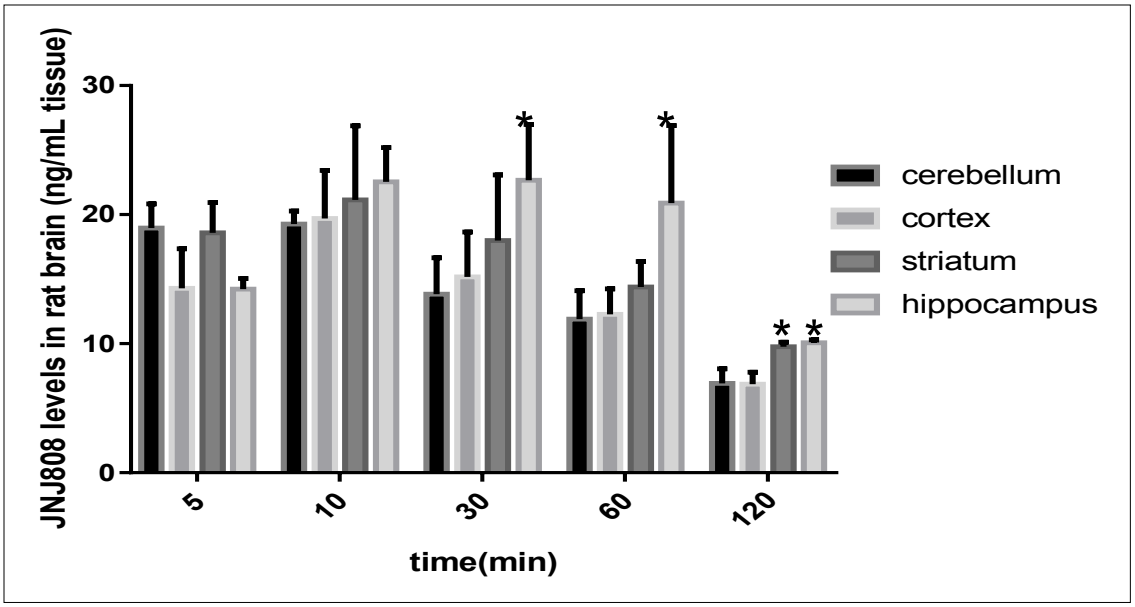

Figure 4. Biodistribution of **12** in rat brain regions at different time points after a single i.v. injection of 30 μg/kg. All animals were sacrificed at different time points (5, 10, 30, 60 and 120 min after the injection). The result is normalized by tissue weight (g). *P<0.05 significant increased vs. cerebellum. N=3.

The synthesis of **12** on gram scale was conducted beginning from 6-bromo-1,3-dihydro-imidazo[4,5-*b*]pyridin-2-one (Scheme 2). It should be noted that this route was chosen in part due to the immediate availability of ethyl 6-bromo-2-oxo-2,3-dihydro-imidazo[4,5-*b*]pyridine-1-carboxylate in house. In order to achieve the desired protecting group positioning on the core beginning with 6-bromo-1,3-dihydro-imidazo[4,5-*b*]pyridin-2-one,

a carbamate protecting group was selectively installed using ethyl pyridine-2-yl carbonate, which was followed by trityl protection of the 3-position *N*-H. The ethyl carbamate was then deprotected with isopropylamine and the resulting *N*-H was subjected to S_N2 reaction conditions with 1-(azetidin-1-yl)-2-chloroethan-1-one. Finally, a Suzuki coupling followed by trityl deprotection and *N*-methylation provided **12.**

Scheme 2. Multi-gram route for compound **12**.[a]

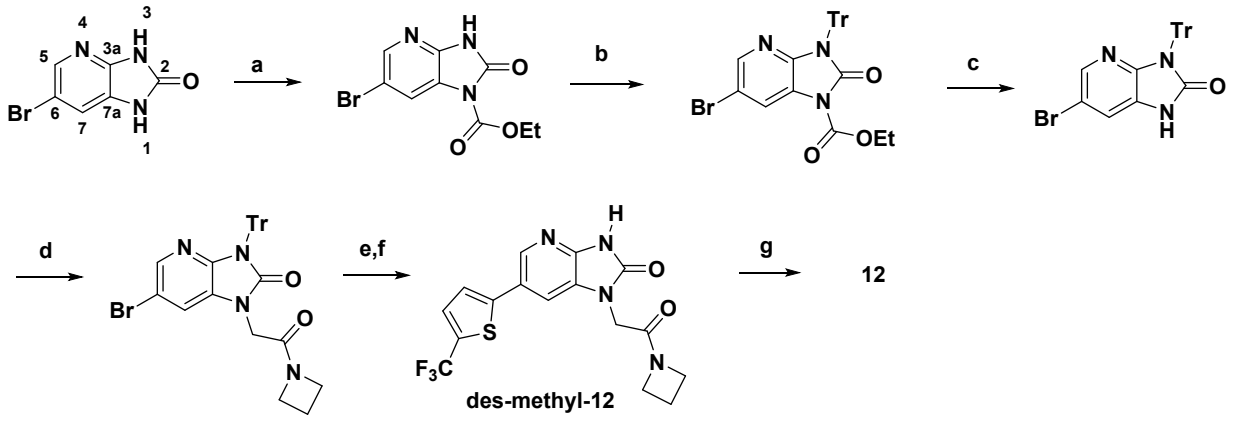

[a] Reagents and conditions: (a) ethyl pyridin-2-yl carbonate, potassium carbonate, DMF, 75 °C (93%); (b) trityl chloride, triethylamine, rt (94%); (c) isopropylamine, THF, rt (100%); (d) sodium hydride, DMF, rt, 20 min; then 1-(azetidin-1-yl)-2-chloroethan-1-one, DMF, rt, 2 h (100%); (e) Boronic Acid, cesium carbonate, $PdCl_2$(dppf), dioxane, 100 °C, 16 h; (f) TFA, CH_2Cl_2, rt, 2h (64% over 2 steps); (g) sodium hydride, DMF, rt, 30 min; then iodomethane, DMF, rt, 2 h (80%).

The dose dependency of **12** was obtained from GluN2B rat hippocampal occupancy measurements after oral administration at 8 different doses (Table 3 and Figure 5). Receptor occupancy was determined at 60 min post dose (3 animals per group), by ex vivo ARG.[29] The calculations were made vs naïve control as described for the 6 hour time course (vide supra). The 60 min time point measurement was chosen based on the t_{max} from the rat PK experiment. Compound **12** occupied the receptor in rat hippocampus with a plasma EC_{50} of 407 ng/mL and a corresponding ED_{50} of 0.86 mg/kg (Figure 5). The receptor occupancy we targeted in order to both produce desired pharmacology and have the potential to minimize unwanted CNS effects[15] was 70% for 1-2 h. The total plasma concentration (bound + unbound) required to achieve 70% occupancy was 716 ng/mL (95% confidence interval 558 to 919 ng/mL).

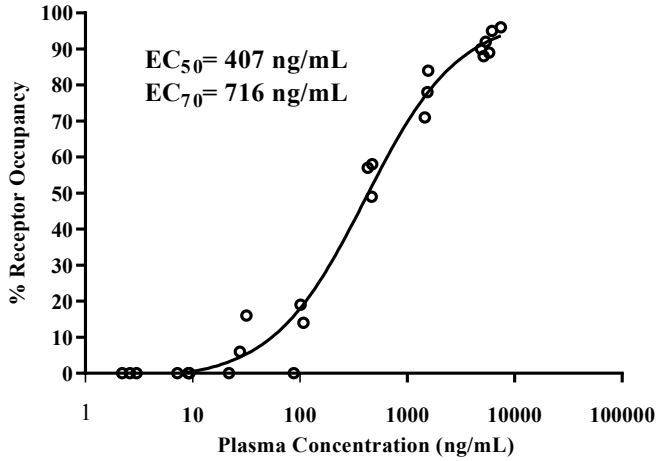

A

B

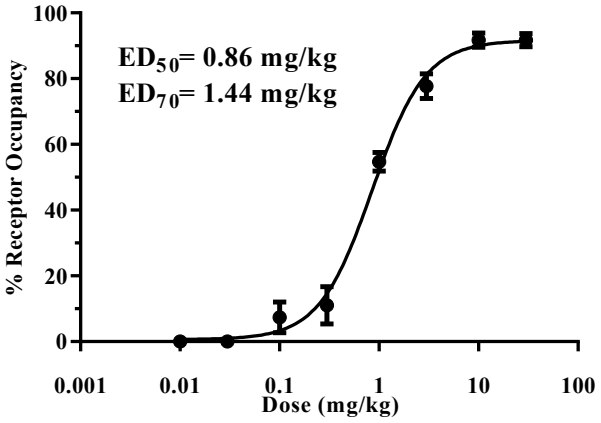

Figure 5. Ex Vivo GluN2B receptor occupancy with **12** in rat hippocampus: dose dependency after p.o. administration shown as (A) Plasma concentration vs % GluN2B occupancy, and (B) Dose v.s. % GluN2B occupancy. Results are expressed as average

percentage receptor occupancy *vs*. naïve control rats ± SEM (n=3) and vehicle is 20% HP-β-CD.

The in vitro profile of compound **12** is shown (Table 4). The unbound fraction in human and rat plasma was 4.6% and 5.3%, respectively, giving an unbound plasma EC_{70} for **12** of 40 ng/mL in rat (based on total bound + unbound plasma EC_{70} = 716 ng/mL). Compound **12** displayed no significant inhibition of cytochrome P450s (CYP) 3A4, 1A2, 2C19, 2C8 or 2C9 up to 50 μM, and no time-dependent inhibition of CYP3A4. It was found to be a moderate inhibitor of CYP2D6 with an IC_{50} of 15 μM. It showed no induction of CYP3A4 or CYP1A2. Compound **12** did not inhibit the hERG channel at any concentration assessed. It did not have any appreciable effect in a radioligand binding assay screen against a panel of 50 targets (GPCRs, ion channels, and transporters) at a concentration of 10 μM.

Table 4. In vitro ADME and selectivity data for compound **12.**

GluN2B rat [a] / human	16 ± 7 /

K_i [b] (nM)		15 ± 6
GluN2- A / C / D IC_{50}[c]		>10 μM
h / rat / dog / mky CL_{int} microsomes[d] μL/min/mg		5.4 / 26.3 / 14.7 / 16.6
CYP isoform IC_{50} (for IC_{50} < 50 μM)[e]		2D6 (15 μM)
3A4 time-dependent inhibition		no [f]
CYP induction		no [g]
Solubility	pH 4	<4

(μM)	pH 7	<4
	SGF	4.4
	SIF	8.4
hERG QPatch™ IC_{50}		>30 μM
h / r plasma protein (% free @ 0.5 μM)[h]		4.6 / 5.3

[a] Ki values were determined using a radioligand competitive binding assay in rat cortex membranes using ([^{3}H]-1-(azetidin-1-yl)-2-(6-(4-fluoro-3-methylphenyl)-1H-pyrrolo[3,2-b]pyridin-1-yl)ethanone.[29] Values reported are the mean of three experiments ± SD, unless otherwise stated. [b] K_i measured in cortical neurons. [c]IC_{50} values are reported in nM and were determined by a calcium mobilization assay in inducible CHO T-Rex cells heterologously expressing the hGluN1a/GluN2A, hGluN1a/GluN2C or hGluN1a/GluN2D receptor. [d] Stability in human and rat liver microsomes. Data reported as microsomal extraction ratio. [e] CYP IC_{50} values were obtained from human liver microsomes for six isoforms: 1A2, 2C19, 2C8, 2C9, 2D6, 3A4. [f] No CYP3A4 inhibition was measured up to 10 μM of **12** either with or without 30 min pre-incubation. [g] Showed <20% activation of human PXR (CYP3A) or AhR (CYP1A), compared to rifampicin and omeprazole, respectively. [h] Equilibrium dialysis method.

Preclinical PK data for **12** is shown in Table 5. The i.v. PK was characterized by low CL in monkey (9 mL/min/kg) and moderate CL in mouse, rat and dog (54, 30 and 17

mL/min/kg, respectively). The CL values were reasonably well predicted in vitro from liver microsomes, except for monkey, which had lower in vivo CL than predicted from in vitro (Table 4). Compound **12** had moderate V_{ss} in preclinical species ranging from 0.8 to 3.2 L/kg. A short i.v. half life was observed in all species ($0.2 \leq t_{1/2} \geq 1.1$ h). Oral bioavailability was moderate in dog (43%) and monkey (41%), moderately high in mouse (69%), and high in rat (132%) (Tables 2 and 5).

Table 5. In vivo PK measurements of **12** in dog, monkey, rat and mouse, n=3 per dose ± SD.

Species	Dose		i.v.				p.o.				
	iv	po	Cl (mL/min/kg)	V_{ss} (L/kg)	$t_{1/2}$ (h)	AUC_{inf}	C_{max} (ng/mL)	AUC_{inf} (hr·ng/mL)	t_{max}	$t_{1/2}$	%F
dog	0.1	0.5	17±9	0.8 ±0.2	0.8 ±0.3	126 ±81	351 ±28	268±42	0.25 ±0.0	0.7 ±0.0	43 ±7
monkey	0.1	0.5	9±2	0.8 ±0.1	1.1 ±0.2	190 ±46	167 ±19	385±14	1.0 ±0.0	1.0 ±0.0	41 ±1

rat	0.5	2.5	30±0.9	1.9 ±0.1	0.8 ±0.0	277±8	479 ±172	1829 ±535	1.3 ±0.6	2.2 ±0.3	132 ±39
mouse	0.5[a]	2.5	54	3.2	0.9	156	413 ±84	539±3	0.3 ±0.1	2.4 ±0.6	69 ±0.0

[a] For the i.v. arm, n=2 animals

Next, **12** was evaluated in a single day dose ranging study in rats, in order to establish doses for an extended 14-day toleration study. The solubility of **12** was assessed and was found to be <<10 mg/mL in 18 organic enabling excipients (and < 1 mg/mL in 30% SBE-β-CD, 50% PEG-400, and 20% HP-β-CD). The poor solubility observed in the excipients assessed did not provide a path forward in supporting rat toleration studies. Given this limitation, high dose single day oral PK studies in rat were conducted using a suspension formulation (5% hydroxypropyl methylcellulose (HPMC)). Compound **12** was administered by oral gavage formulated in HPMC to groups of 3 male Sprague Dawley rats at single dose levels of 125, 250, 500 and 1000 mg/kg in rat, and blood samples were collected at 6 time points ranging from 0.5 to 24 h. The resulting maximum plasma

concentrations ranged from 4237 ± 585 ng/mL at 125 mg/kg to 7010 ± 1058 ng/mL at 1000 ng/mL (Figure 6).

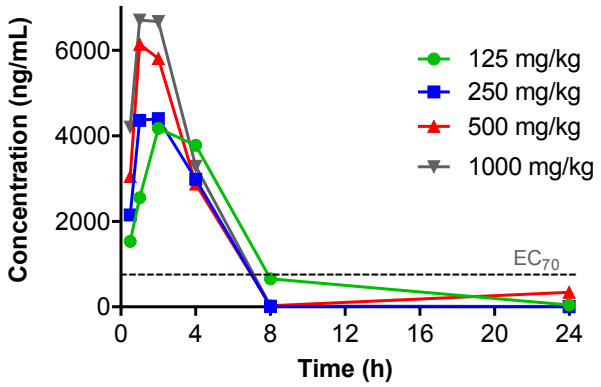

Figure 6. Rat plasma concentrations of **12** over 24 h after four toleration doses administered as oral suspensions in 5% HPMC, n=3. Error bars have been omitted for clarity.

Unfortunately, maximum plasma levels in the single day dose ranging study in rat were less than 10-fold over the EC_{70} for **12**, which would provide insufficient margins to properly assess its nonclinical safety and tolerability.

In order to overcome the poor solubility and/or inadequate dissolution rate of **12** in vivo, a nanosuspension formulation was next developed. Given its poor aqueous solubility,

relatively high melting point (237 °C) and high crystallinity, we recognized that if a stable nanocrystal formulation could be accessed, **12** plasma exposures could be improved with p.o. dosing if 1) low observed exposures were due to limited absorption of **12**, and 2) poor absorption was due to insufficient dissolution rates of **12**. Since the rate of dissolution of a solid drug is directly proportional to particle size (available surface area), if points 1) and 2) are valid, and the intrinsic solubility of the API is at a critical minimum level, the dissolution rate in the gastrointestinal tract may be increased enough to translate into higher overall plasma exposures. Compound **12** was wet-milled with HPMC polymer (API:polymer=4:1) to give a mean particle size of d=0.10649 μm (D90=0.1195; D10=0.0827). The particle size data obtained on the stock solution after milling and again after storing the formulated product under refrigerated conditions for 5 days was stable; no agglomeration or particle growth was observed.

The nanosuspension stock solution was then diluted with vehicle on the day of dosing to support rat studies at 100, 250, and 500 mg/kg. Compound **12** nanosuspension was administered by oral gavage to groups of 3 male Sprague Dawley rats at each dose level, and blood samples were collected at time points ranging from 0.5 to 24 h. In this case,

the resulting maximum plasma exposures after nanosuspension p.o. delivery was dose-dependent, with maximum exposures at 500 mg/kg (Figure 7). Compared to the standard suspension exposures, the C_{max} was three-fold higher using nanosuspension delivery, and $AUC_{0\text{-}24\ h}$ was >5-fold higher (Table 6).

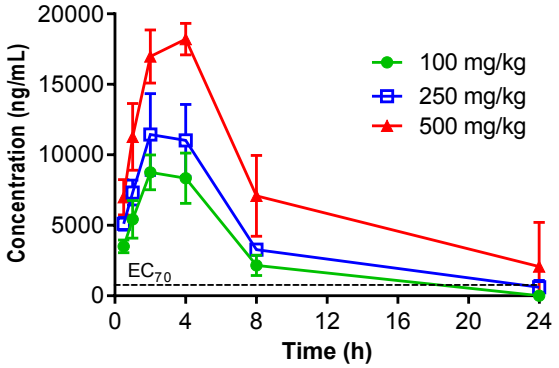

Figure 7. Rat plasma concentrations of **12** over 24 h after toleration doses administered as oral nanosuspensions (API:polymer=4:1), n=3 per dose ± SD.

Table 6. Comparison of rat plasma C_{max}, T_{max} and AUC of **12** administered as a nanosuspension orally at toleration doses versus a standard suspension administered orally at 500 mg/kg.

Suspension particle size	dose (mg/kg)	C_{max} (ng/mL)	T_{max} (hr)	$AUC_{0\text{-}24\ h}$ (hr*ng/mL)	C_{max}/ EC_{70}

nano	100	8996± 1539	2.7±1.2	51858±10524	13x
	250	12451±2288	2.7±1.2	86378±5156	17x
	500	18274±1196	3.3±1.2	156267±40536	26x
standard	125	4237± 685	2.7±1.2	22777±10809	6x
	250	5477±1157	2.7±1.2	19729±5370	8x
	500	6141 ± 271	1.0±0.0	22537 ± 5277	9x
	1000	7010±1058	2.3±1.5	22276±6154	10x

Compound **12** was next tested in rat repeated dose toleration studies using the nanosuspension formulation. In rats, the initial high dose toxicokinetic (TK) study of the nanosuspension described above was followed by a second single dose study that

included a 1,000 mg/kg group. Plasma drug exposures were similar among rats dosed 500 or 1,000 mg/kg; therefore, 500 mg/kg/day was selected as the high dose in the 14-day repeated dose phase of the study.

In the 14-day arm of the study, the most significant clinical observations in the high dose group were aggressive behavior after 2 days. The animals were moved to individual caging on Day 6, and no dose-limiting toxicity was identified up to 500 mg/kg/day for 14 days. At the end of the study, a dose of 500 mg/kg/day correlated to C_{max} and $AUC_{0\text{-}24\ h}$ values of 21,700 and 222,000 h×ng/mL, respectively; the C_{max} is 31-fold over the EC_{70} for **12**.

In order to estimate the human dose which would be predicted to provide 1-2 h coverage of **12** above its EC_{70}, a systemic PK model for **12** was developed using a physiologically-based pharmacokinetic (PBPK) modeling and simulation software (GastroPlus™ 9.0, Simulations Plus, Lancaster, CA). This model predicted a human V_{ss} of 0.95 L/kg. For human CL predictions were attempted by several mechanistic methods and ultimately the most consistent across species was a prediction from measured in vitro data in liver microsomes (intrinsic clearance [CL_{int}]) without any binding corrections (Table 7).

Table 7. Human clearance prediction summary for **12**.

Species	*In vivo* plasma CL (mL/min/kg)	*In vivo* blood CL[a] (mL/min/kg)	Predicted CL (mL/min/kg)		
			Method 1[b]	Method 2[c]	Method 3[d]
human	-	-	0.6	4.6	3.2
dog	17	25	1.6	13	-
monkey	9.1	9.1	4.1	20	-
rat	30	25	1.5	15	-
mouse	54	36	6.3	45	-

[a] Blood CL calculated as plasma CL/blood to plasma ratio
[b] Well-stirred model using in vitro CL_{int} with microsomal and plasma protein binding corrections (GastroPlus default scaling method)
[c] Well-stirred model with no binding corrections: $CL = CL_{int} \times Q/(CL_{int} + Q)$, where Q - species specific hepatic blood flow (21, 31, 44, 70 and 150 mL/min/kg in human, dog, monkey, rat and mouse, respectively)
[d] 4-species allometry with maximum life span correction

This approach provided consistent CL predictions across species within a ~2.2 fold range from the observed in vivo values. The predicted human CL from this method was 4.6 mL/min/kg. Using 4 species allometric scaling (dog, monkey, rat, and mouse) and unbound CL with the Maximum Lifespan Potential (MLP) correction, the estimated human CL value was 3.2 mL/min/kg. These two methods provided fairly similar predictions, however, the value of 4.6 (more conservative) was further used in human PK profile simulations.

The plasma exposure over time profile in human was simulated by GastroPlus using a combination of the PBPK model and a gastrointestinal (GI) absorption model (ACATTM) developed based on data from oral nanosuspension PK experiments in dog. Simulations were conducted in order to predict plasma levels above the calculated 70% effective concentration (EC_{70}) of 716 ng/mL for approximately 1.5 h (Table 8 and Figure 8), which resulted in a predicted C_{max} of 904 ng/mL. The C_{max} on day 14 of the rat toleration study (21,700 ng/mL) versus the human predicted C_{max} (904 ng/mL) represents a 24-fold margin. The human predicted AUC_{inf} was 4127 hr*ng/mL, which compared to the day 14 $AUC_{0\text{-}24h}$ of the maximum tolerated dose in rat (222,000 hr*ng/mL), represents a 53-fold AUC margin.

Table 8. Predicted human PK parameters for **12** using PKPD plus GI absorption models.

oral dose (mg)	Cl (mL/min/kg)	V_{ss} (L/kg)	$t_{1/2}$ (h)	C_{max} (ng/mL)	AUC_{inf} (hr*ng/mL)	%F
120	4.6	0.95	2.4	904	4127	67

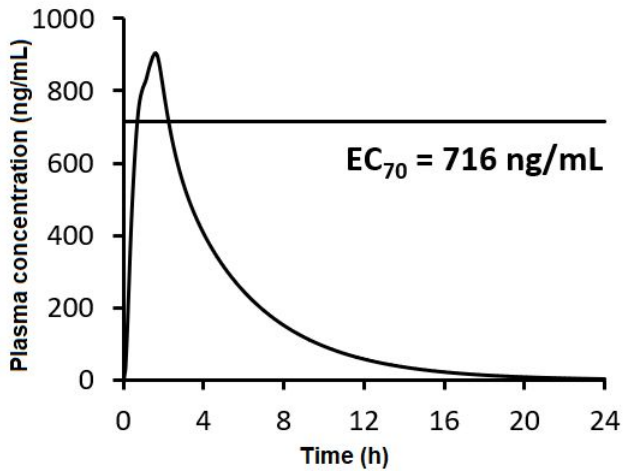

Figure 8. Simulated human plasma concentration profile 120 mg of a single oral dose of **12** from a nanosuspension formulation.

CONCLUSIONS:

In summary, we have identified a structurally novel class of GluN2B modulators containing a 1,3-dihydro-imidazo[4,5-*b*]pyridin-2-one core system. These compounds in general had poor aqueous solubility, but were prioritized because they demonstrated low turnover in liver microsomes. The poor solubility translated into slow dissolution rates and limited absorption in rats at high doses. As a result, lead compound **12** at high doses formulated in HPMC did not lead to high enough plasma concentrations in rat toleration

studies to provide an acceptable margin above the plasma EC_{70} value of 716 ng/mL needed to assess its safety. A stable nanosuspension formulation was subsequently developed in order to address this challenge. The nanosuspension enabled toleration studies with **12** which achieved a 24-fold C_{max} margin (highest plasma concentration of the maximum tolerated dose on day 14 in rat versus the highest human predicted plasma concentration) and a 53-fold AUC margin. Compound **12** was shown to have high receptor occupancy after oral administration with an ED_{70} of 1.4 mg/kg in rat, as measured by ARG. Subsequent to this work, compound **12** was progressed into advanced good laboratory practice (GLP) studies, the results of which shall be disclosed in due course.

EXPERIMENTAL SECTION:

Chemistry General Methods. Solvents and reagents were used as supplied by the manufacturer. Concentrated refers to concentrated using a rotary evaporator under reduced pressure.

Unless specified otherwise, normal-phase silica gel column chromatography (FCC) was performed on silica gel (SiO_2) using prepackaged cartridges and the indicated

solvents. Preparative reverse-phase high performance liquid chromatography (HPLC) was performed under one of three conditions:

1) An Agilent HPLC with a Waters XBridge C18 column or Xterra Prep RP_{18} column (5 µm, 30x100 mm or 50x150 mm) and a gradient of 5-99% acetonitrile/water (20 mM NH_4OH) over 12 to 18 min and a flow rate of 30 or 80 ml/min.

2) A Shimadzu LC-8A Series HPLC with an XBridge C18 OBD column (5 µm, 50 x 100mm), mobile phase of 5% ACN in H_2O (both with 0.05% TFA) was held for 1 min, then a gradient of 5-99% ACN over 14 min, then held at 99% ACN for 10 min, with a flow rate of 80 mL/min.

3) A Shimadzu LC-8A Series HPLC with an Inertsil ODS-3 column (3 µm, 30 x 100mm, T = 45 °C), mobile phase of 5% ACN in H_2O (both with 0.05% TFA) was held for 1 min, then a gradient of 5-99% ACN over 6 min, then held at 99% ACN for 3 min, with a flow rate of 80 mL/min.

HRMS was obtained on an Agilent G6230B Time-of-Flight (TOF) mass spectrometer, using a Dual AJS ESI in positive mode with a scan range of 100-1700 amu. The TOF was tuned using Agilent Technologies ESI-L Low Concentration Tune Mix

(G1969-85000). This was diluted 10x with 90% acetonitrile in water and to this mixture, 5 uL of 0.1 mM hexamethoxy-phosphazine (HP-0321) was added. The reference mass solution was made using the Agilent Technologies ES-TOF Reference Mass Solution Kit (G1969-85001), which contains 100 mM ammonium trifluoroacetate ($TFANH_4$), 5mM purine, and 2.5 mM hexakis (1H, 1H, 3H-tetrafluoropropoxy)phosphazine (HP-0921), all in 90:10 acetonitrile: water. The solution was made by adding 0.1 mL $TFANH_4$, 0.4 mL purine, and 1.0 mL HP-0921 to 1 L of 95:5 acetonitrile:water. This reference solution was continuously infused during the run. Samples were run through an ACE-3 C18 column (3μm, 35 x 2.1 mm), with a mobile phase of 10-98% acetonitrile in 0.01% formic acid over 2 min and then held at 98% acetonitrile for 1 min, at a flow rate of 0.300 mL/min.

Nuclear magnetic resonance (NMR) spectra were obtained on Bruker model DRX spectrometers. Chemical shifts (δ) are expressed in parts per million, relative to internal tetramethylsilane; coupling constants (J) are in hertz (Hz). Measurements were made using 5 mm tubes.

All compounds tested were of a minimum of 95% purity as determined by HPLC. The HPLC method used for purity determinations is as follows: Analytical LCMS was obtained

on an Agilent 1100 Series using an ACE C18 column (3µm, 3.0 x 50mm, T = 50 °C) with a mobile phase of with a mobile phase of 5-99% ACN in 0.05% TFA over 1.5 min and then hold at 99% ACN for 0.5 min, at a flow rate of 2.2 mL/min. MS detector is an Agilent G1956B MSD set in positive mode. Alternatively, compound purity was assessed on a Waters Classic Acquity system using a Waters Acquity UPLC BEH C18 column (1.7 µm, 2.1x50mm, T = 65 °C) with a mobile phase of 5-95% ((9:1=water:10 mM NH_4Ac)/ACN)/ MeOH over 1.7 min and then hold at 95% MeOH for 0.3 min, at a flow rate of 0.7 mL/min.The MS detector is a Waters SQ Detector (set in positive/negative mode).

Preparation of 2-(6-bromo-3-methyl-2-oxo-2,3-dihydro-imidazo[4,5-b]pyridin-1-yl)acetic acid (20). *Step 1. 5-bromo-N-methyl-3-nitropyridin-2-amine.* To a solution of 5-bromo-2-chloro-3- nitropyridine (15 g, 63 mmol) in THF (570 mL) at 0°C was added a solution of methylamine (40% in H_2O, 10.9 mL, 126 mmol). The reaction mixture was stirred at room temperature for 16 h. Upon completion, the reaction mixture was extracted with EtOAc (3 x 500 mL). The combined organic layers were dried (Na_2SO_4), filtered and concentrated under reduced pressure to yield the title compound as a yellow solid (14.6 g, 62.7 mmol, 99%), which was used in the next step without further purification. ^{1}H NMR (500 MHz,

DMSO-d_6) 8.54 (d, J = 2.3 Hz, 1H), 8.46 (d, J = 2.3 Hz, 1H), 8.17 (bs, 1H), 3.16 (d, J = 4.9 Hz, 3H). MS (ESI): mass calcd. for $C_6H_6BrN_3O_2$, 230.96; m/z found, 232 $[M+H]^+$.

Step 2. 5-bromo-N²-methylpyridine-2,3-diamine. To a stirred suspension of 5-bromo-N-methyl-3-nitropyridin-2-amine (14.6 g, 62.7 mmol) and zinc (41 g, 627 mmol) in a mixture of water (29 mL) and acetone (291 mL) was added NH_4Cl (33.6 g, 627 mmol). The reaction mixture was stirred at room temperature for 72 h. Upon completion the mixture was filtered through Celite ® and rinsed with DCM. The filtrate was washed with water and the aqueous layer was extracted with DCM (3X). The combined organic layers were dried (Na_2SO_4), filtered and concentrated under reduced pressure to yield the title compound as an oil (12.7 g, 62.8 mmol, 100%), which was used in the next step without further purification. MS (ESI): mass calcd. for C H BrN , 200.99; m/z found, 202 $[M+H]^+$.

*Step 3. 6-bromo-3-*methyl*-1,3-dihydro-imidazo[4,5-b]pyridin-2-one (**18**).* To a solution of 5-bromo-N²-methylpyridine-2,3-diamine (14 g, 69 mmol) in DMF (702 mL) at room temperature was added CDI (29 g, 180 mmol). The reaction mixture was stirred for 16 h. LCMS analysis of the crude reaction mixture showed that the reaction was not complete, and the resulting residue was re-dissolved in THF and CDI (11.2 g, 69 mmol) was added.

The reaction mixture was stirred at 60°C for 16 h. The reaction mixture was quenched with water and diluted with ether. The suspension was filtered and the resulting solid was washed with ether then dried under vacuum to yield the title compound as a black solid (15.8 g, 35.7 mmol, 52%), which was used in the next step without further purification. MS (ESI): mass calcd. for $C_7H_6BrN_3O$, 226.97; m/z found, 227.0 [M+H] +.

*Step 4. ethyl 2-(6-bromo-3-methyl-2-oxo-2,3-dihydro-imidazo[4,5-b]pyridin-1-yl)acetate (**19**).* Under a nitrogen atmosphere was added **18** (5 g, 21.9 mmol) to a suspension of sodium hydride (60% dispersion in mineral oil, 1.3 g , 32.9 mmol) in DMF (171 mL) at room temperature. After 10 minutes ethyl bromoacetate (3.2 mL, 28.5 mmol) was added and the reaction was stirred at room temperature. After 4 h, complete conversion was observed. The reaction was cooled to 0 °C and water was added (200 mL). The precipitates were collected by filtration and washed with water to give the title compound (6.1 g, 19.2 mmol, 88%). ^{1}H NMR (500 MHz, DMSO-d_6) δ 8.14 (d, J = 2.0 Hz, 1H), 7.92 (d, J = 2.0 Hz, 1H), 4.76 (s, 2H), 4.16 (q, J = 7.1 Hz, 2H), 3.35 (s, 3H), 1.22 (t, J = 7.1 Hz, 3H). MS (ESI): mass calcd. for $C_{11}H_{12}BrN_3O_3$, 313.0; m/z found, 313.9 [M+H] +.

*Step 5. 2-(6-bromo-3-*methyl*-2-oxo-2,3-dihydro-imidazo[4,5-b]pyridin-1-yl)acetic acid (20)*. Lithium hydroxide (2M, 1.2 mL, 2.3 mmol) was added to a mixture of **19** (612 mg, 1.9 mmol) in THF (23 mL) at room temperature. The precipitates were collected by filtration and washed with THF to give the title compound (465 mg, 2.0 mmol, 83%). ^{1}H NMR (500 MHz, DMSO-d_6) δ 8.02 (d, J = 2.0 Hz, 1H), 7.46 (d, J = 2.0 Hz, 1H), 4.03 (s, 2H), 3.31 (s, 3H). MS (ESI): mass calcd. for $C_9H_8BrN_3O_3$, 285.0; m/z found, 286.0 [M+H]+.

General Amide Formation Procedure (21-23). A mixture of **20** (1 equiv), Amine (1.1 equiv), Hunig's base (2 equiv), T3P® (50% solution in DMF, 3 equiv) in DMF or DCM (0.1 M) was stirred at rt or 50°C. After reaction completion as indicated by consumption of starting material by LCMS, the reaction mixture was cooled to room temperature and a saturated aqueous solution of $NaHCO_3$ (20 mL) was added. The mixture was extracted using DCM (3 x 30 mL). The combined organics were dried over $MgSO_4$, filtered and concentrated. The crude product was purified by FCC (SiO_2, 0-100% EtOAc in hexanes) or prep HPLC to give **21-23**.

*2-(6-bromo-3-methyl-2-oxo-2,3-dihydro-imidazo[4,5-b]pyridin-1-yl)-N,N-dimethylacetamide (**21**)* (504 mg, 61%). ^{1}H NMR (400 MHz, DMSO-d_6) δ 8.12 - 8.08 (d, *J* = 2.0 Hz, 1H), 7.81 - 7.77 (d, 2.0 Hz, 1H), 4.83 4.75 (s, 2H), 3.35 3.33 (s, 3H), 3.08 - 3.06 (s, 3H), 2.85 - 2.83 (s, 3H). MS (ESI): mass calcd for $C_{11}H_{13}BrN_4O_2$, 313.1 m/z found, 314.1 $[M+H]^+$.

1-(2-(azetidin-1-yl)-2-oxoethyl)-6-bromo-3-methyl-1,3-dihydro-imidazo[4,5-b]pyridin-2-one (**22**) (179 mg, 78%). ^{1}H NMR (500 MHz, DMSO-d_6) δ 8.10 (d, *J* = 2.0 Hz, 1H), 7.78 (d, *J* = 2.0 Hz, 1H), 4.55 (s, 2H), 4.27 (t, *J* = 7.6 Hz, 2H), 3.91 (t, *J* = 7.7 Hz, 2H), 3.33 (s, 3H), 2.32 - 2.24 (m, 2H). MS (ESI): mass calcd for $C_{11}H_{13}BrN_4O_2$, 325.1 m/z found, 326.1 $[M+H]^+$.

6-bromo-1-(2-(3-fluoroazetidin-1-yl)-2-oxoethyl)-3-methyl-1,3-dihydro-imidazo[4,5-b]pyridin-2-one (**23**), (435 mg, 73%). ^{1}H NMR (500 MHz, DMSO—d_6) δ 8.1 1 (d, *J* = 2.0 Hz, 1H), 7.79 (d, *J* = 2.0 Hz, 1H), 5.55 - 5.38 (m, 1H), 4.67 - 4.57 (m, 3H), 4.45 - 4.33 (m , 1H), 4.30 - 4.18 (m, 1H), 4.03 3.91 (m, 1H), 3.34 (s, 3H). MS (ESI): mass calcd for $C_{12}H_{12}BrF_4O_2$, 342.0 m/z found, 342.8 $[M+H]^+$.

General Procedure A for Suzuki Coupling (5-7). A mixture of Aryl Bromide (**21-23**) (1 equiv), Boronic Acid (2 equiv), $PdCl_2$(dppf).DCM (0.07 equiv), Cs_2CO_3 (2 equiv) and dioxane (1.1 mL) sealed in a microwave vial under a nitrogen atmosphere was heated to 100°C using an oil bath. After 16 h, the reaction mixture was cooled to rt to afford the crude compound. The crude product was dissolved in MeOH and purified by preperative HPLC to afford the desired compound.

*1-(2-(azetidin-1-yl)-2-oxoethyl)-3-methyl-6-(3-(trifluoromethyl)phenyl)-1,3-dihydro-imidazo[4,5-b]pyridin-2-one (**5**)*. General Suzuki Coupling Procedure A using **22** (6 mg, 10%). ^{1}H NMR (500 MHz, DMSO-d_6) δ 8.40 (d, *J* = 2.0 Hz, 1H), 8.04 - 7.97 (m, 2H), 7.90 (d, *J* = 2.0 Hz, 1H), 7.78 - 7.69 (m, 2H), 4.63 (s, 2H), 4.29 (t, *J* = 7.7 Hz, 2H), 3.91 (t, *J* = 7.7 Hz, 2H), 3.40 (s, 3H), 2.33 - 2.24 (m, 2H). ^{13}C NMR (151 MHz, $CDCl_3$) δ 166.02, 159.45, 159.17, 158.90, 153.74, 143.05, 138.70, 138.60, 131.85, 131.64, 131.43, 131.21, 130.67, 130.47, 129.63, 124.90, 124.72, 124.60, 124.58, 124.55, 124.53, 124.00, 123.98, 123.95, 123.93, 123.09, 115.88, 114.50, 113.98, 77.23, 77.02, 76.81, 50.74, 48.98, 40.81, 26.73, 15.72. HRMS (ESI) calcd. for $C_{19}H_{17}F_3N_4O_2$ $[M+H]^+$ 390.1320, found 391.1390.

*N,N-dimethyl-2-(3-methyl-2-oxo-6-(3-(*trifluoromethyl*)phenyl)-2,3-dihydro-imidazo[4,5-b]pyridin-1-yl)acetamide (**6**)*. General Suzuki Coupling Procedure A using **21** (7 mg, 9%). ^{1}H NMR (400 MHz, DMSO-d_6) δ 8.40 (d, J = 2.0 Hz, H), 8.03 7.96 (, 2H), 7.90 (d, J = 2.0 Hz, 1H), 7.77 7.69 (m, 2H), 4.87 (s, 2H), 3.40 (s, 3H), 3.1 1 (s, 3H), 2.85 (s, 3H). HRMS (ESI) calcd. for $C_{16}H_{15}F_3N_4O_2S$ $[M+H]^+$ 384.3, found 385.1.

*1-(2-(3-*fluoroazetidin*-1-yl)-2-oxoethyl)-3-methyl-6-(3-(trifluoromethyl)phenyl)-1,3-dihydro-imidazo[4,5-b]pyridin-2-one* (**7**). General Suzuki Coupling Procedure A using **23** (19 mg, 31%). ^{1}H NMR (400 MHz, DMSO-d_6) δ 8.40 (d, J = 1.9 Hz, 1H), 8.02 - 7.97 (m, 2H), 7.89 (d, J = 2.0 Hz, 1H), 7.78 - 7.70 (m, 2H), 5.58 - 5.37 (m, 1H), 4.76 - 4.57 (m, 3H), 4.47 - 4.34 (m, 1H), 4.31 - 4.18 (, 1H), 4.04 - 3.90 (m, 1H), 3.40 (s, 3H). ^{13}C NMR (151 MHz, $CDCl_3$) δ 166.14, 153.78, 143.48, 139.57, 139.06, 131.62, 131.41, 130.80, 130.32, 129.63, 124.93, 123.13, 113.99, 82.41, 81.04, 77.23, 77.02, 76.80, 58.38, 58.20, 56.70, 56.53, 41.43, 26.45. HRMS (ESI) calcd. for $C_{19}H_{16}F_4N_4O_2$ $[M+H]^+$ 408.1222, found 409.1296.

N,N-dimethyl-2-(3-methyl-6-(4-methylthiophen-2-yl)-2-oxo-2,3-dihydro-imidazo[4,5-b]pyridin-1-yl)acetamide (**10**). General Suzuki Coupling Procedure A using **21** (48 mg,

46%). ^{1}H NMR (400 MHz, $CDCl_3$) δ 8.30 - 8.27 (d, *J* = 1.9 Hz, H), 7.35 - 7.31 (d, *J* = 1.9 Hz, H), 7.08 - 7.04 (d, *J* = 1.4 Hz, 1H), 6.88 - 6.84 (m, 1H), 4.76 - 4.66 (s, 2H), 3.55 - 3.49 (s, 3H), 3.20 - 3.14 (s, 3H), 3.04 – 2.96 (s, 3H), 2.33 - 2.25 (d, *J* = 1.1 Hz, 3H). ^{13}C NMR (151 MHz, $CDCl_3$) δ 165.8, 154.1, 143.3, 140.9, 138.7, 125.9, 125.3, 124.4, 120.3, 112.3, 77.2, 77.1, 76.8, 42.4, 36.7, 35.9, 26.2, 15.8. HRMS (ESI) calcd. for $C_{16}H_{18}N_4O_2S$ $[M+H]^+$ 330.1160, found 331.1233.

*1-(2-(azetidin-1-yl)-2-*oxoethyl*)-3-methyl-6-(5-methylthiophen-2-yl)-1,3-dihydro-imidazo[4,5-b]pyridin-2-one (**11**).* General Suzuki Coupling Procedure A using **22** (17 mg, 23%). ^{1}H NMR (500 MHz, $CDCl_3$) δ 8.27 - 8.25 (d, *J* = 1.9 Hz, 1H), 7.40 - 7.38 (d, *J* = 1.9 Hz, 1H), 7.06 - 7.04 (d, *J* = 3.5 Hz, 1H), 6.75 - 6.72 (m, 1H), 4.50 - 4.46 (s, 2H), 4.32 - 4.27 (m, 2H), 4.12 - 4.06 (m, 2H), 3.53-3.49 (s, 3H), 2.53 - 2.49 (d, *J* = 1.1 Hz, 3H), 2.39 - 2.31 (m, 2H). ^{13}C NMR (151 MHz, $CDCl_3$) δ 165.81, 153.78, 142.78, 139.97, 138.49, 138.04, 126.26, 125.64, 124.25, 123.56, 112.37, 77.23, 77.02, 76.81, 50.51, 48.65, 40.92, 26.35, 15.76, 15.42. HRMS (ESI) calcd. for $C_{17}H_{18}N_4O_2S$ $[M+H]^+$, 342.1169, found 343.1243.

Compounds **12**-**14** were prepared from **19** using General Procedure A followed by ester hydrolysis as described for **19** → **20**. The last step can be conducted using General Amide Formation Procedure.

For in vivo receptor occupancy and PK studies, compounds **12-14** were prepared using an alternative route.

Synthetic route for in vivo receptor occupancy and PK studies of 12-14.

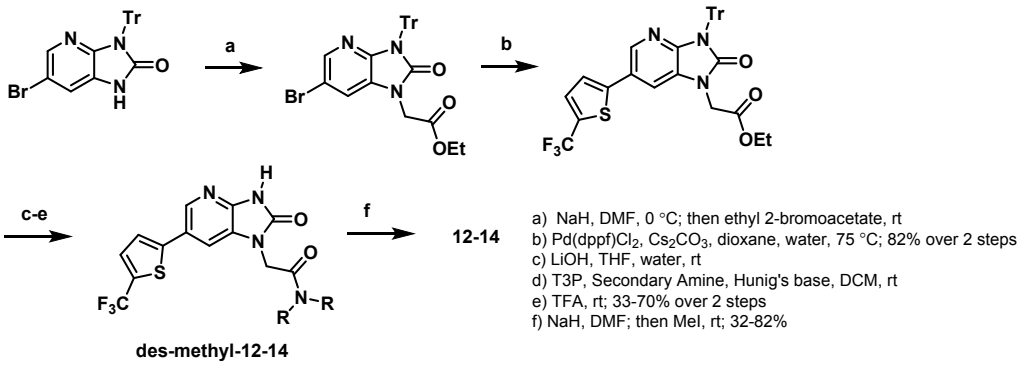

2-(2-oxo-6-(5-(trifluoromethyl)thiophen-2-yl)-3-trityl-2,3-dihydro-imidazo[4,5-b]pyridin-1-yl)acetic acid. *Step 1. 6-bromo-1,3-dihydro-imidazo[4,5-b]pyridin-2-one.* To a solution of 2,3-diamino-5-bromopyridine (5 g, 27 mmol) in THF (87 mL) was added CDI (3.02 g, 18.6 mmol), and the reaction mixture was stirred at 80°C for 6 h. Then, water was added and the mixture was filtered. The solids were collected by filtration, washed with water and ether, and dried under vacuum to afford the title compound (5.3 g, 25 mmol, 93%),

which was used in the next step without further purification. MS (ESI): mass calcd. for $C_6H_4BrN_3O$, 212.95 m/z found, 214 $[M+H]^+$.

Step 2. Ethyl 6-bromo-2-oxo-2,3-dihydro-imidazo[4,5-b]pyridine-1-carboxylate. A mixture of 6-bromo-1,3-dihydro-imidazo[4,5-*b*]pyridin-2-one (5.3 g, 25 mmol), ethyl pyridin-2-yl carbonate (5.36 g , 27.2 mmol) and K_2CO_3 (3.77 g , 27.2 mmol) in DMF (245 mL) was heated to 75 °C for 3 h . The crude reaction mixture was concentrated in vacuo and diluted with water and 1 M HCl until the mixture reached pH 1. The solution was filtered and triturated with ether to afford the title compound (6.6 g, 23 mmol, 93%), which was used in the next step without further purification. MS (ESI): mass calcd. for $C_9H_8BrN_3O_3$, 284.97 m/z found, 286 [M+H]+.

Step 3. Ethyl 6-bromo-2-oxo-3-trityl-2,3-dihydro-imidazo[4,5-b]pyridine-1-carboxylate. To a solution of ethyl 6-bromo-2-oxo-2,3-dihydro-imidazo[4,5-*b*]pyridine-1-carboxylate (8.0 g, 11.8 mmol) in DCM (25 mL) at rt was added trityl chloride (5.36 g, 19.2 mmol) followed by Et_3N (2.1 g, 21.0 mmol). The mixture was stirred at room temperature for 16 h then concentrated. To the residue was added water (100 mL) and extracted with EtOAc (3x50 mL). The combined organic layers were dried with Na_2SO_4, filtered and

concentrated to yield the title compound as an amorphous solid (8.0 g, 68%). ^{1}H NMR (500 MHz, $CDCl_3$) δ 8.15 (d, *J* = 2.1 Hz, 1H), 7.90 (d, *J* = 2.2 Hz, 1H), 7.54-7.43 (m, 6H), 7.25-7.14 (m, 9H), 4.47 (q, *J* = 7. Hz, 2H), 1.42 (t, *J* =7.1 Hz, 3H).

Step 4: 6-Bromo-3-trityl-1,3-dihydro-imidazo[4,5-b]pyridin-2-one. A mixture of ethyl 6-bromo-2-oxo-3-trityl-2,3-dihydro-imidazo[4,5-b]pyridine-1-carboxylate (3.7 g, 7.0 mmol) and isopropylamine (0.72 mL, 8.4 mmol) in THF (35 mL) was stirred at room temperature for 2 h. Then, the reaction mixture was concentrated under vacuum to yield the title compound as a yellow oil (3.2 g, 7.0 mmol, 100%), which was used without further purification. ^{1}H NMR (400 MHz, $CDCl_3$) δ 8.87 (s, 1H), 7.80 (d, *J* = 2.1 Hz, 1H), 7.55 – 7.44 (m, 5H), 7.34 – 7.14 (m, 10H), 7.10 (d, *J* = 2.1 Hz, 1H).

Step 5. 1-(2-(azetidin-1-yl)-2-oxoethyl)-6-bromo-3-trityl-1,3-dihydro-imidazo[4,5-b]pyridin-2-one. Under a nitrogen atmosphere was added NaH (60% dispersion in mineral oil, 1.03 g, 25.8 mmol) to a stirring solution of 6-bromo-3-trityl-1,3-dihydro-imidazo[4,5-*b*]pyridin-2-one (5.67 g, 12.3 mmol) in DMF (40 mL). After 20 minutes, 1-(azetidin-1-yl)-2-bromoethan-1-one (2.84 g, 15.9 mmol) in DMF (10 mL) was added to the reaction mixture. After 2 h, the reaction mixture was poured into ice water (500 mL). The

precipitates were collected by suction filtration and isolated as a white solid (6.79 g, 12.3 mmol, 100%).^{1}H NMR (400 MHz, $CDCl_3$) δ 7.82 (d, *J* = 2.0 Hz, 1H), 7.52 – 7.44 (m, 6H), 7.28 (d, J = 2.1 Hz, 1H), 7.31 – 7.12 (m, 9H), 4.35 (s, 2H), 4.02 (t, *J* = 7.8 Hz, 2H), 3.82 (t, *J* = 7.7 Hz, 2H), 3.70 (s, 2H), 2.26 – 2.15 (m, 1H).

*Step 6. 1-(2-(azetidin-1-yl)-2-oxoethyl)-6-(5-(trifluoromethyl)thiophen-2-yl)-1,3-dihydro-imidazo[4,5-b]pyridin-2-one (***des-methyl-12***).* To a mixture of 1-(2-(azetidin-1-yl)-2-oxoethyl)-6-bromo-3-trityl-1,3-dihydro-imidazo[4,5-b]pyridin-2-one (6.79 g, 12.3 mmol), 5-(trifluoromethyl)thiophen-2-ylboronic acid (2.64 g, 13.5 mmol), Cs_2CO_3 (7.99 g, 24.5 mmol) and $PdCl_2$(dppf).DCM (610 mg, 0.75 mmol) in a 500 mL rb flask under N_2 was added dioxane (100 mL). The reaction was stirred at 75 °C for 16 hours under N_2. The reaction was cooled to room temperature and diluted with EtOAc (100 mL) and water (200 mL). The layers were separated and the water layer was extracted with DCM (2 x 100 mL). The combined organic layers were dried using $MgSO_4$, filtered and concentrated under vacuum. The crude material was purified (FCC, SiO_2, 0-100% EtOAc in hexanes) to afford 5.3 g of while solid (1-(2-(azetidin-1-yl)-2-oxoethyl)-6-(5-(trifluoromethyl)thiophen-2-yl)-3-trityl-1,3-dihydro-imidazo[4,5-*b*]pyridin-2-one.) The solid

was diluted in DCM (100 mL) and TFA was added (50 mL). The mixture was stirred for 2h at rt, then the solvents were removed in vacuo, following which DCM (200 mL) and sat $NaHCO_3$ (200 mL) were added. The resulting solids were collected by suction filtration. The mother liquor layers were separated, and the water layer was extracted with DCM (3x100 mL). The combined organic layers were dried using $MgSO_4$, filtered and concentrated under vacuum, and purified by FCC (0-10% {7N NH_3 in MeOH}/DCM) to afford a white solid, which was combined with the first crop of solids to afford the title compound (3.01 g, 7.87 mmol, 64% over 2 steps). ^{1}H NMR (500 MHz, DMSO-d_6) δ 11.85 (s, 1H), 8.34 (d, *J* = 2.0 Hz, 1H), 7.79 (d, *J* = 2.0 Hz, 1H), 7.76 (dq, *J* = 3.9, 1.3 Hz, 1H), 7.58 (dt, *J* = 3.8, 1.3 Hz, 1H), 4.54 (s, 2H), 4.28 (t, *J* = 7.7 Hz, 2H), 3.91 (t, *J* = 7.7 Hz, 2H), 2.29 (p, *J* = 7.8 Hz, 2H). MS (ESI): mass calcd. for $C_{16}H_{13}F_3N_4O_2S$, 382.3 m/z found, 383.0.

*Step 7. 1-(2-(azetidin-1-yl)-2-oxoethyl)-3-*methyl*-6-(5-(trifluoromethyl)thiophen-2-yl)-1,3-dihydro-imidazo[4,5-b]pyridin-2-one (**12**).* To a solution of **des-methyl-12** (3.0 g, 7.8 mmol) in DMF (80 mL) was added NaH (60% dispersion in mineral oil, 377 mg, 9.42 mmol) in one portion at room temperature. Vigorous bubbling occurred and the reaction

was stirred until gas evolution had ceased (30 min), then iodomethane (0.73 mL, 11.8 mmol) was added and the reaction mixture was stirred at room temperature for an additional 2h. The reaction was poured into ice water (400 mL). The resulting solids were collected by suction filtration and washed with water (200 mL). The mother liquor was extracted with EtOAc (8x100 mL). The combined organic layers were dried over Na_2SO_4, filtered. To this solution was added the filtered solids and 30 g silica gel. The solvents were removed to dryness and the residue was purified on 300 g silica column (FCC, 0-10% {7N NH_3 in MeOH}/DCM) to afford the title compound (2.5 g, 6.3 mmol, 80%). Mp 237.40-237.87 °C. ^{1}H NMR (400 MHz, $CDCl_3$) δ 8.32 (d, *J* = 1.9 Hz, 1H), 7.46 (d, *J* = 1.9 Hz, 1H), 7.43 (dq, *J* = 3.7, 1.1 Hz, 1H), 7.21 (dq, *J* = 3.7, 1.1 Hz, 1H), 4.51 (s, 2H), 4.36 (t, *J* = 7.8 Hz, 2H), 4.11 (t, *J* = 7.8 Hz, 2H), 3.55 (s, 3H), 2.43-2.35 (m, 2H). ^{19}F NMR (376 MHz, $CDCl_3$) δ -55.34. ^{13}C NMR (101 MHz, $CDCl_3$) δ 165.56, 153.75, 145.16, 143.99, 138.72, 129.46, 129.42, 124.42, 123.64, 123.19, 112.78, 77.35, 77.23, 77.03, 76.71, 50.47, 48.62, 40.70, 26.39, 15.73. MS (ESI) calcd. for $C_{17}H_{15}F_3N_4O_2S$ $[M+H]^+$ 396.1, found 397.1.

Synthesis of 13-14 from 6-Bromo-3-trityl-1,3-dihydro-imidazo[4,5-b]pyridin-2-one.

Step 1. Ethyl 2-(6-bromo-2-oxo-3-trityl-2,3-dihydro-imidazo[4,5-b]pyridin-1-yl)acetate. Under a nitrogen atmosphere was added 6-bromo-3-trityl-1,3-dihydro-imidazo[4,5-*b*]pyridin-2-one (3.2 g , 7.0 mmol) to a suspension of NaH (60% dispersion in mineral oil, 393 mg, 9.8 mmol) in DMF (50 mL). After 20 minutes, ethyl bromoacetate (0.18 mL, 1.6 mmol) was added to the reaction mixture. After 2 h, the reaction mixture was quenched with water (200 mL). The precipitates were filtered off and isolated as a white solid.(3.8 g, 7.0 mmol, 99%). ^{1}H NMR (500 MHz, DMSO-d_6) δ 7.86 (d, *J* = 2.1 Hz, 1H), 7.81 (d, *J* = 2.1 Hz, 1H), 7.43 – 7.39 (m, 6H), 7.25 – 7.20 (m, 6H), 7.19 – 7.13 (m, 3H), 4.68 (s, 2H), 4.08 (q, *J* = 7.1 Hz, 2H), 1.12 (t, *J* = 7.1 Hz, 3H).

Step 2. Ethyl 2-(2-oxo-6-(5-(trifluoromethyl)thiophen-2-yl)-3-trityl-2,3-dihydro-imidazo[4,5-b]pyridin-1-yl)acetate. A mixture of ethyl 2-(6-bromo-2-oxo-3-trityl-2,3-dihydro-imidazo[4,5-b]pyridin-1-yl)acetate (230 mg, 0.4 mmol), 4,4,5,5-tetramethyl-2-(5-(trifluoromethyl)thiophen-2-yl)-1,3,2-dioxaborolane (153 mg, 0.6 mmol), Cs_2CO_3 (240 mg, 0.7 mmol) and $PdCl_2$(dppf).DCM (21 mg, 0.06 mmol) in dioxane (3.5 mL) was combined in a microwave vial and stirred in a 75°C oil bath. The reaction mixture was stirred at 75°C for 16 hours then cooled down to room temperature and quenched with a saturated

aqueous solution of $NaHCO_3$. The resulting reaction mixture was extracted with EtOAc (3 x 60 mL) and the combined organic layers were dried using MgS04, filtered and concentrated under vacuum. The crude material was purified (FCC, SiO_2, 0-40% EtOAc in hexanes) to afford the title compound. (215 mg, 0.4 mmol, 82%). ^{1}H NMR (500 MHz, $CDCl_3$) δ 7.97 - 7.95 (d, *J* = 2.1 Hz, 1H), 7.45 - 7.40 (m, 6H), 7.30 7.27 (m, 1H), 7.19 - 7.14 (m, 6H), 7.14 - 7.09 (m, 3H), 7.04 - 7.03 (d, *J* = 2.0 Hz, 1H), 7.03 - 7.00 (m, 1H), 4.49 - 4.45 (s, 2H), 4.17 - 4.10 (m, 2H), 1.19 - 1.15 (m, 3H).

Step 3. 2-(2-oxo-6-(5-(trifluoromethyl)thiophen-2-yl)-3-trityl-2,3-dihydro-imidazo[4,5-b]pyridin-1-yl)acetic acid. To a solution of ethyl 2-(2-oxo-6-(5-(trifluoromethyl)thiophen-2-yl)-3-trityl-2,3-dihydro-imidazo[4,5-b]pyridin-1-yl)acetate (1.0 g, 1.8 mmol) in THF (1 mL) and MeOH (1 mL) at room temperature was added LiOH (53 mg, 2.2 mmol) in water (0.033 mL, 1.8 mmol)). The mixture was stirred for 5 h then concentrated in vacuo to a white solid (1.03 g, 1.8 mmol, contains water). The solids were used in the next step without further characterization.

General Amide Formation Procedure followed by trityl deprotection (des-methyl 13-14). A mixture of 2-(2-oxo-6-(5-(trifluoromethyl)thiophen-2-yl)-3-trityl-2,3-dihydro-imidazo[4,5-

b]pyridin-1-yl)acetic acid (1 equiv), Amine (1.1 equiv), Hunig's base (2 equiv), T3P® (50% solution in DCM, 3 equiv) in DCM (0.1 M) was stirred at rt for 16 h. The reaction mixture was concentrated under reduced pressure and the residue was purified (FCC, SiO_2, 0-100% EtOAc in hexanes). To the EA/hexanes solution containing the product was added 1 mL TFA. The resulting reaction mixture stirred at room temperature for 16 hours. The excess TFA was evaporated under reduced pressure and the crude material was purified (FCC, SiO_2,0-15% 2M NH_3/MeOH in DCM) to afford the desired compound.

*N,N-dimethyl-2-(2-oxo-6-(5-(trifluoromethyl)thiophen-2-yl)-2,3-dihydro-imidazo[4,5-b]pyridin-1-yl)acetamide (**Des-methyl-13**),* (25 mg, 33%). ^{1}H NMR (500 MHz, DMSO-d_6) δ 11.8 - 11.7 (s, 1H), 8.34 - 8.32 (d, *J* = 2.0 Hz, 1H), 7.79 - 7.76 (s, 1H), 7.76 - 7.74 (d, *J* = 3.7 Hz, 1H), 7.57 7.55 (s, 1H), 4.80 - 4.75 (s, 2H), 3.10 (s, 3H), 2.85 (s, 3H). MS (ESI): mass calcd. for $C_{15}H_{13}F_3N_4O_2S$, 370.1 m/z found, 371 .0.

*1-(2-(3-fluoroazetidin-1-yl)-2-oxoethyl)-6-(5-(trifluoromethyl)thiophen-2-yl)-1,3-dihydro-imidazo[4,5-b]pyridin-2-one (**Des-methyl-14**),* (108 mg, 70%). MS (ESI): mass calcd. for $C_{16}H_{12}F_4N_4O_2S$, 400.1 m/z found, 401.0.

General Procedure for *N*-Methylation (13-14). To a solution of **des-methyl-13** or **des-methyl-14** (1 equiv) in DMF (2 mL) was added NaH (60% dispersion in mineral oil, 1.2 equiv) in one portion at room temperature. The reaction was stirred until gas evolution had ceased, then iodomethane (1.5 equiv) was added. The mixture was stirred at room temperature overnight then diluted with water. The aqueous layer was extracted with EtOAc. The combined organic layers were dried over Na_2SO_4, filtered and concentrated under reduced pressure. The crude solid was purified (FCC, SiO_2, 0-50% IPA in EtOAc in DCM) to yield **13-14**.

N,N-dimethyl-2-(3-methyl-2-oxo-6-(5-(trifluoromethyl)thiophen-2-yl)-2,3-dihydro-imidazo[4,5-b]pyridin-1-yl)acetamide (**13**), (37 mg, 82%). ^{1}H NMR (400 MHz, $CDCl_3$) δ 8.30 (d, *J* = 1.9 Hz, 1H), 7.43 – 7.38 (m, 1H), 7.34 (d, *J* = 2.0 Hz, 1H), 7.20 – 7.15 (m, 1H), 4.72 (s, 2H), 3.53 (s, 3H), 3.18 (s, 3H), 3.00 (s, 3H). ^{13}C NMR (151 MHz, $CDCl_3$) δ 165.62, 154.04, 145.42, 144.27, 138.88, 129.44, 129.41, 124.64, 123.53, 123.12, 112.50, 77.24, 77.02, 76.81, 42.41, 36.67, 35.89, 26.32. HRMS (ESI) calcd. for $C_{16}H_{15}F_3N_4O_2S$ $[M+H]^+$ 384.0883, found 385.0953.

1-(2-(3-fluoroazetidin-1-yl)-2-oxoethyl)-3-methyl-6-(5-(trifluoromethyl)thiophen-2-yl)-1,3-dihydro-imidazo[4,5-b]pyridin-2-one (**14**), (279 mg, 32%). ^{1}H NMR (500 MHz, $CDCl_3$) δ 8.33 - 8.30 (d, *J* = 1.9 Hz, 1H), 7.44 7.43 (d, *J* = 1.9 Hz, 1H), 7.43 7.40 (m, 1H), 7.21 - 7.18 (m, 1H), 5.45 - 5.28 (m, 1H), 4.68 - 4.12 (m, 7H), 3.55 - 3.50 (s, 3H). ^{13}C NMR (151 MHz, $CDCl_3$) δ 165.98, 153.71, 145.06, 144.02, 138.97, 130.27, 129.49, 129.46, 124.26, 123.77, 123.29, 112.73, 82.35, 80.98, 77.23, 77.02, 76.81, 58.27, 58.09, 56.62, 56.44, 41.11, 26.45. HRMS (ESI) calcd. for $C_{17}H_{14}F_4N_4O_2S$ $[M+H]^+$ 414.0790, found 415.0863.

General Procedure B for Suzuki Coupling (15-17). To a solution of the corresponding 2-bromo-5-substituted-thiophene (3 equiv) in dioxane (3 mL) was added bis(pinacolato)diboron (4 equiv), KOAc (12 equiv), and $PdCl_2$(dppf).DCM (0.5 equiv). The resulting reaction mixture was stirred at 90°C for 2 hours under a nitrogen atmosphere. The reaction mixture was then cooled to room temperature and **22** (1 equiv) was added followed by Cs_2CO_3 (3 equiv), dioxane (2 mL) and again $PdCl_2$(dppf).DCM (0.5 equiv). The reaction mixture was stirred at 90°C for an additional 2 hours under a nitrogen atmosphere. The reaction was cooled to room temperature and washed with water. The organic layer was dried with $MgSO_4$ and concentrated and the residue was purified by

FCC (SiO_2, 0-7% 2M NH_3/MeOH in DCM) followed by basic HPLC (Agilent) to provide the desired compound.

1-(2-(azetidin-1-yl)-2-oxoethyl)-6-(5-(difluoromethyl)thiophen-2-yl)-3-methyl-1,3-dihydro-imidazo[4,5-b]pyridin-2-one (**15**), (56 mg, 48%). ^{1}H NMR (500 MHz, $CDCl_3$) δ 8.33 - 8.27 (d, *J* = 2.0 Hz, 1 H), 7.47 - 7.40 (d, *J* = 2.1 Hz, 1H), 7.28 - 7.24 (m, 1H), 7.21 - 7.15 (m, 1H), 6.96 - 6.68 (t, *J* = 56.1 Hz, 1H), 4.53 - 4.43 (s, 2H), 4.38 - 4.25 (m, 2H), 4.12 - 4.05 (m, 2H), 3.55 - 3.50 (s, 3H), 2.43 - 2.26 (m, 2H). ^{13}C NMR (151 MHz, $CDCl_3$) δ 165.65, 153.80, 144.26, 143.83, 138.77, 135.65, 135.48, 135.31, 128.58, 128.53, 128.49, 124.36, 124.20, 123.19, 113.05, 112.71, 111.48, 109.92, 77.23, 77.02, 76.81, 50.49, 48.64, 40.76, 26.34, 15.75. HRMS (ESI) calcd. for $C_{17}H_{16}F_2N_4O_2S$ $[M+H]^+$ 378.0976, found 379.1050.

1-(2-(azetidin-1-yl)-2-oxoethyl)-6-(4-(difluoromethyl)thiophen-2-yl)-3-methyl-1,3-dihydro-imidazo[4,5-b]pyridin-2-one (**16**), (35.5 mg, 20%). ^{1}H NMR (500 MHz, $CDCl_3$) δ 8.30 - 8.28 (d, *J* = 1.9 Hz, 1H), 7.51 - 7.47 (m, 1H), 7.45 7.41 (d, *J* = 1.9 Hz, 1H), 7.35 - 7.32 (d, *J* = 1.3 Hz, 1H), 6.81 - 6.54 (m, 1H), 4.51 4.45 (s, 2H), 4.37 4.29 (m, 2H), 4.13 - 4.06 (m, 2H), 3.55 - 3.48 (s, 3H), 2.41 2.30 (m, 2H). ^{13}C NMR (151 MHz, $CDCl_3$) δ 165.72,

153.82, 143.71, 143.17, 138.72, 137.18, 137.02, 136.85, 124.57, 124.52, 124.47, 124.32, 124.29, 120.83, 120.80, 120.78, 113.15, 112.56, 111.58, 110.01, 77.24, 77.03, 76.82, 50.51, 48.66, 40.75, 26.30, 15.75. HRMS (ESI) calcd. for $C_{17}H_{16}F_2N_4O_2S$ $[M+H]^+$ 378.0975, found 379.1048.

1-(2-(azetidin-1-yl)-2-oxoethyl)-6-(5-cyclopropylthiophen-2-yl)-3-methyl-1,3-dihydro-imidazo[4,5-b]pyridin-2-one (**17**), (11 mg, 10%). ^{1}H NMR (500 MHz, $CDCl_3$) δ 8.26 - 8.23 (d, *J* = 1.8 Hz, 1H), 7.39 - 7.37 (d, *J* = 1.9 Hz, 1H), 7.05 - 7.01 (d, *J* = 3.6 Hz, 1H), 6.75 6.71 (m , 1H), 4.50 - 4.44 (s, 2H), 4.32 - 4.24 (m, 2H), 4.12 - 4.05 (m, 2H), 3.52 - 3.49 (s, 3H), 2.38 - 2.28 (m, 2H), 2.12 - 2.04 (m, 1H), 1.05 - 0.97 (m, 2H), 0.80 - 0.72 (m, 2H). ^{13}C NMR (151 MHz, $CDCl_3$) δ 165.88, 153.87, 148.83, 142.91, 138.37, 137.38, 125.61, 124.13, 123.73, 123.28, 112.19, 77.23, 77.02, 76.81, 50.51, 48.65, 40.93, 26.22, 15.74, 11.28, 9.82. HRMS (ESI) calcd. for $C_{19}H_{20}N_4O_2S$ $[M+H]^+$ 368.1319, found 369.1393.

Calcium mobilization (FLIPR) assay. CHO-T-Rex cells expressing Biomyx hNR1a/NR2 clones (BIOMYX Inc., San Diego, CA): Cells are grown to 75-90% confluence before passaging. Cells are lifted using 0.05% Trypsin/EDTA solution. Each confluent T225 flask typically yields enough cells for 2 plates (384-well) at the plating density of 20,000

cells/50µl/well. Twenty-four hours before measurements, the expression of the NMDA receptors in the stable cell line is induced with Tet-On inducible system in the presence of ketamine, a non-selective NMDA receptor blocker. On the day of the experiment, cell culture media is carefully washed and the cells are loaded with Calcium 5 Dye Kit (Molecular Devices) in dye loading buffer containing 137 mM NaCl, 4 mM KCl, 2 mM $CaCl_2$, 0.5 mM $MgCl_2$, 10 mM HEPES and 5 mM D-glucose; pH 7.4. After 1h incubation at the room temperature, the dye is washed away with the assay buffer (137 mM NaCl, 4 mM KCl, 2 mM $CaCl_2$, 0.01 mM EDTA, 10 mM HEPES and 5 mM D-glucose; pH 7.4) In the FLIPR TETRA reader, various concentrations of the test compounds are added to the cells for 5 min while fluorescence is monitored to detect potential agonist activity. Next, co-agonists, glutamate and glycine are added for another 5 minutes. The concentration of glutamate corresponding to ~EC_{80} is used to maximize the assay's signal window and ability to detect NMDA receptor antagonists and negative allosteric modulators. A saturating concentration (10 µM) of glycine is also present in the assay. A non-selective NMDA receptor antagonist, (+)MK-801 is used as a positive control for antagonist activity. The fluorescent signal in the presence of test compounds is quantified and normalized to

the signal defined by the appropriate control wells. Experiments were performed three independent times in duplicate except for compounds **5**-**7**, which were assayed in two independent experiments in duplicate.

Radioligand binding assay. Rat adult cortex is homogenized in the assay buffer (50 mM Tris; pH 7.4). The resulting cortical membranes containing native NMDA receptors are purified by centrifugation and extensively washed, then re-suspended in the assay buffer. The test compounds, 3-[^{3}H] 1-(azetidin-1-yl)-2-[6-(4-fluoro-3-methyl-phenyl)pyrrolo[3,2-*b*]pyridin-1-yl]ethanone[29] and membranes are mixed together and incubated with shaking for 2 hours at room temperature to reach binding equilibrium. Non-specific binding of 3-[^{3}H] 1-(azetidin-1-yl)-2-[6-(4-fluoro-3-methyl-phenyl)pyrrolo[3,2-*b*]pyridin-1-yl]ethanone is determined by pre-incubation of brain membranes with 10 μM of **2** (CP-101,606). Following the incubation, the bound and unbound tracer is separated by filtration with cell harvester and GF/B filter plates (PerkinElmer) soaked with polyethylenimine. The extent of binding is measured by counting [^{3}H] radioactivity retained on the filters plates with liquid scintillator counter. Binding affinity (equilibrium dissociation constant K_i) for the test compounds is determined by fitting experimental data with the following model

logEC50=log(10^logKi*(1+[Radioligand]/HotKd)) and Y=Bottom + (Top-Bottom)/(1+10^(X-LogEC50)) where [Radioligand] is the concentration of 3-[^{3}H] 1-(azetidin-1-yl)-2-[6-(4-fluoro-3-methyl-phenyl)pyrrolo[3,2-*b*]pyridin-1-yl]ethanone, HotKdNM is the equilibrium dissociation constant of 3-[^{3}H] 1-(azetidin-1-yl)-2-[6-(4-fluoro-3-methyl-phenyl)pyrrolo[3,2-*b*]pyridin-1-yl]ethanone, Top and Bottom are the curve plateaus in the units of Y axis. Experiments were performed three independent times in duplicate with the exception of compounds **6** and **16**, which were assayed in two independent experiments in duplicate.

Solubility in Aqueous Systems. The solubility of **12** in aq buffer (pH 2 and pH 7), simulated gastric and intestinal fluids was conducted as previously described.[36]

Liver Microsomal Stability. Microsomal stability studies were conducted in duplicate as previously described.[36]

MDCK/MDR-1 Permeability. Permeability assays were conducted at Cyprotex according to the company's protocol using the MDCK-MDR1 cell line obtained from the NIH. In brief, cells between passage numbers 6 – 30 were seeded onto a Multiscreen plate™ (Millipore) at a cell density of 3.4 x 10^5 cells/cm^2 and cultured for three days before

permeability studies were conducted. Test compounds were dissolved as 10 mM DMSO solutions and added to Hanks Balanced Salt Solution (HBSS), pH 7.4 culture media at a final concentration of 5 μM (1 % DMSO v/v). The working solution was applied to cells on the donor side and incubated at 37° C for 60 min to determine the apical (A) to basolateral (B) and B to A permeability, respectively. In addition, A to B permeability was measured in the presence of the PgP inhibitor elacridar (2 μM). All conditions for test compound were conducted in duplicate, and each assay includes the reference markers propranolol (high permeability) and prazosin (PgP substrate). After incubation, samples were processed for LC/MS/MS analyses to determine the apparent permeability coefficient (Papp) of the test compound in the A to B direction in the presence and absence of the PgP inhibitor and in the B to A direction. In addition, the percent recovery was measured for all incubation conditions. The integrity of each monolayer was monitored by examining the permeation of lucifer yellow by fluorimetric analysis.

Plasma Protein Binding. Plasma protein binding for **12** was determined using the equilibrium dialysis method as previously described in triplicate.[36] The parent compound recovery at the end of the experiment was ≥100%.

Inhibition of CYP450s by 12 using probe substrates. The potential of compound **12** to inhibit human CYPs was investigated via incubating specific CYP probe substrates (Table 2 in SI) with human liver microsomes in the presence of **12** as previously described[37] at various concentrations up to 20 μM (solubility limit). The IC_{50} values for various CYPs were determined by measuring the effect of **12** on the metabolite formation by probe substrate and are reported as the mean of two independent experiments. Known specific CYP inhibitors were used as positive controls to monitor the assay performance. Compound **12** at concentrations up to 20 μM did not show significant inhibition of CYPs, except CYP2D6 for which moderate inhibition with an IC_{50} value of 15 μM was observed (Table 2 of SI). The possibility of clinically significant drug-drug interactions due to inhibition of other CYPs by **12** is considered low.

CYP3A4 Time-dependent Inhibition. CYP3A4 inhibition was determined in human liver microsomes both with and without 30 min preincubation of various concentrations of **12** (0.4 to 10 μM) by the previously described method.[37] The IC_{50} values of CYP3A4 activity are calculated in this experiment as the average of two independent experiments from the percent CYP3A4 activity remaining after compound incubation at the various

concentrations relative to vehicle. A greater than 2-fold shift in the IC_{50} value as a result of preincubation vs no preincubation was considered a threshold for time-dependent inhibition. For compound **12**, no inhibition was seen either before or after preincubation through the highest concentration tested (10 μM).

CYP450 Induction. The potential of **12** to induce CYPs at the transcriptional level was assessed with the use of the Puracyp (Carlsbad, CA) DPX2 (CYP3A4, pregnane X receptor [PXR]) and DRE (CYP1A, aryl hydrocarbon receptor [AhR]) luciferase-reporter cell line. Rifampicin and omeprazole served as positive controls for CYP3A and 1A induction, respectively. The DPX2 cell line is a derivative of HepG2 cells that is co-transfected with an expression vector containing human PXR and a modified luciferase vector harboring the CYP3A4 promoter. The distal and proximal enhancers are transfected to over-express the PXR. Analogously, the 1A2-DRE stably-transfected cell line harbour the human AhR gene and a Luciferase reporter gene linked to the human CYP1A2 promoter and 3 copies of the dioxin response element (DRE) enhancer. ONE-Glo assay kit from Promega is used to measure the increase in luminescence due to up-

regulation of transfected cell lines, DPX2 or DRE, which are purchased and licensed from Puracyp, Inc.

hERG QPatch™. Experiments were performed using CHO cells stably expressing the hERG potassium channel as previously described.[38] After establishing whole-cell configuration and a stability period, the vehicle was applied for 5 minutes followed by the test substance by increasing concentrations of 0.3, 3.0, 10 and 30 μM. Each concentration of the test substance was applied twice. The effect of each concentration was determined after 5 min as an average current of 3 sequential voltage pulses. To determine the extent of block the residual current was compared with vehicle pre-treatment. Data are presented as mean values ± standard error of the mean (SEM). Compound **12** did not notably affect the membrane potassium current I_{Kr} at 0.3, 3, and 10 μM (1.8%, 1.0%, and 4.2% decrease at 0.3, 3, and 10 μM, respectively, vs. 0.2%, 0.6%, and 2.4% with vehicle), but mildly inhibited I_{Kr} at 30 μM (33.6% inhibition vs. 6.4% with vehicle; IC_{50} >30 μM). No drug exposure analysis was conducted to confirm exposure in this high-throughput screen.

In Vivo Methods. Animal work was done in accordance with the Guide Care for and Use of Laboratory Animals adopted by the US National Institutes of Health. Animals were allowed to acclimate for 7 days after receipt. They were group housed in accordance with institutional standards, received food and water ad libitum and were maintained on a 12 hour light/dark cycle. Male Sprague Daley rats were from Charles River Laboratories or Harlan (Envigo), aged between 8 and 12 weeks and approximately 300-400 grams in body weight. The animals were euthanized using CO_2 and decapitated at the indicated timepoints after drug administration.

Ex vivo radioligand binding autoradiography. For time course studies 2 animals per time point over 3 time points were used. For dose response studies, three animals per dose over 7-10 doses were tested. Brains were rapidly frozen and twenty micron thick tissue sections were prepared for autoradiography (Letavic et al. ACS Med. Chem. Lett., 2013, 4, 419–422). Sections were briefly incubated with the radiotracer 3-[^{3}H] 1-(azetidin-1-yl)-2-[6-(4-fluoro-3-methyl-phenyl)pyrrolo[3,2-*b*]pyridin-1-yl]ethanone.[29] Ex vivo GluN2B labelling was expressed as the percentage of GluN2B labelling in corresponding brain areas of vehicle-treated animals.

Microdosing experiment. To evaluate the brain biodistribution of **12** in rodents at a microdose level, rats (n = 3 each group) were administered with a single intravenous dose of 0.03 mg/kg of compound formulated in 50% (w/v) PEG/water, pH7.4. Animals were sacrificed at 5, 10, 30, 60 and 120 min following the dosing. The cerebellum, cortex, striatum and hippocampus were collected. The sample weight was measured and then homogenized to analyze **17** levels by LC-MS/MS.

LC/MS/MS analysis. Compound **12** was extracted from brain homogenate samples were extracted using a protein precipitation method and analyzed on an API4000 Q-Trap MS/MS System (Applied Biosystems, Concord, Ontario, Canada) interfaced with a Shimadzu HPLC. Samples were loaded onto a 2.1 × 50-mm Gemini, NX-C18, 3 μm 110A column (Phenomenex, Torrance, CA, US) under a flow rate of 0.5 ml/min using water (0.1% formic acid) as mobile phase A and acetonitrile (0.1% formic acid) as mobile phase B. Starting with 85% mobile phase A for 0.5 minutes, mobile phase B was increased from 15% to 98% using a linear gradient for 1.1 minute, held at 98% B for 0.6 minutes, and equilibrated at 15% B for 0.4 minutes for an overall run time of 2.5 minutes. Compound

12 was quantified by MS/MS in the positive ion mode by monitoring the transition of 397 to 312 m/z.

Pharmacokinetic Studies. Single dose pharmacokinetic studies in males Sprague Dawley rats were conducted following i.v. (0.1 or 0.5 mg/kg) and p.o. (0.5 or 2.5 mg/kg) administration as a solution in either 20% HP-β-CD, 50% PEG-400 or 30% SBE-β-CD. Blood was sampled at predose and at 0.033 (iv), 0.083 (iv), 0.25, 0.5, 1, 2, 4, 6, 8, and 24 h postdose. Plasma concentrations were quantitated by LC−MS/MS. Pharmacokinetic parameters were derived from noncompartmental analysis of the plasma concentration vs time data using WinNonlin software (Pharsight, Palo Alto, CA).

Rat toleration studies. For rat toxicokinetic studies, animals (5 per dose group) were administered **12** as a suspension in 5% HPMC or as a stable nanosuspension at doses of 125, 250, 500 and 1000 mg/kg (single dose studies) or 125, 250 and 500 mg/kg (14 Day repeat dose study). Blood samples for toxicokinetics were collected pre-dose and at 1, 2, 4, 7, 24, 48 and 55 h post-dose, and again on day 13 at 0, 1, 2, 4, 7 and 24 h for the repeat dose study. Haematology and clinical chemistry were assessed. Animals were monitored for behavior (daily), body weight (daily) and food consumption (weekly). Gross

pathology and organ weights were assessed on Day 14 autopsy. A selection of harvested tissues were weighed and underwent microscopic examination. Drug plasma concentrations were quantitated by LC−MS/MS. Toxicokinetic parameters were derived from noncompartmental analysis of the plasma concentration vs time data using PKAW R1.0 software.

ASSOCIATED CONTENT

Supporting Information. The Supporting Information is available free of charge via the Internet at http://pubs.acs.org.

Molecular formula strings and IC_{50} data of compounds **10-17** (CSV).

Plasma and brain levels for **12-14** from receptor occupancy time course studies, plasma and brain levels of **12** for dose response receptor occupancy studies, brain levels of **12** in rat from microdosing study, in vitro CL data for **12** in 5 species, CYP450 inhibition data for **12**, solubility results for **12** in enabling excipients, off target selectivity panel data for **12**, and RP-LCMS purity traces for key compounds **11-14**.

AUTHOR INFORMATION

Corresponding Author

*E-mail: cchrovia@its.jnj.com

Author Contributions

The manuscript was written through contributions of all authors. All authors have given approval to the final version of the manuscript.

ACKNOWLEDGMENT

The authors would like to thank Heather Mcallister for HRMS data, Khoa Tran, Compound Logistics LJ and Compound Logistic BE for analytical reports, Yafei Chen and Katie Turner for in vivo protocols, Minerva Batugo and Adam Beaupre for QC and bioanalytical methods, Sangho Yun for formulation studies, and Nick Carruthers and Pascal Bonaventure for helpful suggestions in the preparation of this manuscript.

ABBREVIATIONS

ADME, absorption, distribution, metabolism and excretion, AE, adverse event, AMPA, α-amino-3-hydroxy-5-methyl-4-isoxazolepropionic acid, API, active pharmaceutical

ingredient, AUC, area under the curve, CDI, 1,1'-carbonyldiimidazole, CL, clearance, cLogP, calculated partition co-efficient, CNS, central nervous system, CYP, Cytochrome P450, EC, effective concentration, ED, effective dose, EGTA, ethyleneglycol-bis(2-aminoethylether)-*N,N,N',N'*-tetraacetic acid, ER, extraction ratio, F, bioavailability, FIH, first in human, GLP, good laboratory practice, GPCR, G protein-coupled receptors, HATU, [(Dimethylamino)-1*H*-1,2,3-triazolo-[4,5-*b*]pyridin-1-ylmethylene]-*N*-methylmethanaminium hexafluorophosphate *N*-oxide, HDRS, Hamilton Depression Rating Scale, HEPES, 4-(2-Hydroxyethyl)piperazine-1-ethanesulfonic acid, Het, heterocycle, HP-β-CD, (2-Hydroxypropyl)-β-cyclodextrin, HPMC, hydroxypropyl methylcellulose, HTS, high-throughput screen, IC, inhibitory concentration, iGluR, ionotropic glutamate receptors, i.v., intravenous, LiPE, lipophilic ligand efficiency, MDD, major depressive disorder, NAM, negative allosteric modulator, NMDA, *N*-methyl-*D*-aspartate, NMDAR, *N*-methyl-*D*-aspartate receptor, NOAEL, no adverse event level, PEG400, Polyethylene Glycol 400, PFTBA, perfluorotributylamine, PGP, P-glycoprotein, PK, pharmacokinetics, p.o., per os, PoC, proof of concept, q.d., quaque die (once a

day), SAR, structure-activity relationship, TRD, treatment resistant depression, V_{ss}, volume of distribution.

REFERENCES

(1) Traynelis, S.F.; Wollmuth, L.P.; McBain, C.J.; Menniti, F.S.; Vance, K.M.; Ogden, K.K.; Hansen, K.B.; Yuan, H.; Myers, S.J.; Dingledine, R. Glutamate receptor ion channels: structure, regulation, and function. *Pharmacol Rev.* **2010**, *62*,405-496.

(2) Berberich, S.; Jensen, V.; Hvalby, Ø.; Seeburg, P. H.; Köhr, G. The role of NMDAR subtypes and charge transfer during hippocampal LTP induction. *Neuropharmacology* **2007**, *52*, 77-86.

(3) Massey, P. V.; Johnson, B. E.; Moult, P. R.; Auberson, Y. P.; Brown, M. W.; Molnar, E.; Collingridge, G. L.; Bashir, Z. I. Differential roles of NR2A and NR2B-containing NMDA receptors in cortical long-term potentiation and long-term depression. *J Neurosci*. **2004** ,24, 7821-7828.

(4) Sanacora, G.; Zarate, C. A.; Krystal, J. H.; Manji, H. K. Targeting the glutamatergic system to develop novel, improved therapeutics for mood disorders. *Nat. Rev. Drug Discov*. **2008**, *7*, 426-437.

(5) Duman, R. S.; Sanacora, G.; Krystal, J. H. Altered connectivity in depression: GABA and glutamate neurotransmitter deficits and reversal by novel treatments. *Neuron* **2019**, *102*, 75-90.

(6) Sanacora, G.; Treccani, G.; Popoli, M. Towards a glutamate hypothesis of depression. *Neuropharmacology* **2012**, *62*, 63-77.

(7) Monyer, H.; Sprengel, R.; Schoepfer, R.; Herb, A.; Higuchi, M.; Lomeli, H.; Burnashev, N.; Sakmann, B.; Seeburg, P. H. Heteromeric NMDA receptors: molecular and functional distinction of subtypes. *Science* **1992**, *256*, 1217-1221

(8) Paoletti, P.; Bellone, C.; Zhou, Q. NMDA receptor subunit diversity: impact on receptor properties, synaptic plasticity and disease. *Nat. Rev. Neurosci*. **2013***, 14*, 383-400.

(9) Paoletti, P.; Neyton J. NMDA receptor subunits: function and pharmacology. *Curr Opin Pharmacol.* **2007**, *7*, 39-47.

(10) Nowak, L.; Bregestovski, P.; Ascher, P.; Herbet, A.; Prochiantz, A. Magnesium gates glutamate-activated channels in mouse central neurons. *Nat.* **1984**, *307*, 462-465.

(11) Mayer, M. L.; Westbrook, G. L.; Guthrie, P. B. Voltage-dependent block by magnesium(2+) of NMDA responses in spinal cord neurons. *Nat.* **1984**, *309*, 261-263.

(12) Williams, K. Ifenprodil discriminates subtypes of the N-methyl-D-aspartate receptor: selectivity and mechanisms at recombinant heteromeric receptors. *Mol. Pharmacol.* **1993**, *44*, 851-859.

(13) Carron, M. C. E.; Carron, C. L. C.; Bucher, B. P. 1-(*p*-hydroxyphenyl)-2-(4-alkyl- or -aralkyl-1-piperidino)-1-Propanols Vasodilators. FR 1966-77770, 1966.

(14) Perin-Dureau, F.; Rachline, J.; Neyton, J.; Paoletti, P. Mapping the binding site of the neuroprotectant ifenprodil on NMDA receptors *J.Neurosci.* **2002**, *22*, 5955-5965.

(15) Mony, L.; Kew, J. N. C.; Gunthorpe, M. J.; Paoletti, P. Allosteric modulators of NR2B-containing NMDA receptors: molecular mechanisms and therapeutic potential. *Br. J. Pharmacol*. **2009**, *157*, 1301-1317.

(16) Hashimoto, K., Malchow, B., Falkai P., Schmitt A. Glutamate modulators as potential therapeutic drugs in schizophrenia and affective disorders. *Eur. Arch. Psychiatry Clin. Neurosci.* **2013**, *263*, 367-77.

(17) Preskorn, S. H.; Baker, B.; Kolluri, S.; Menniti, F. S.; Krams, M.; Landen, J. W. An innovative design to establish proof of concept of the antidepressant effects of the NR2B subunit selective N-methyl-D-aspartate antagonist, CP-101,606, in patients with treatment-refractory major depressive disorder. *J. Clin. Psycho-pharm*. **2008**, *28*, 631-637.

(18) Chenard, B. L.; Bordner, J.; Butler, T. W.; Chambers, L. K.; Collins, M. A.; De Costa, D. L.; Ducat, M. F.; Dumont, M. L.; Fox, C. B. (1S,2S)-1-(4-Hydroxyphenyl)-2-(4-hydroxy-4-phenylpiperidino)-1-propanol: a potent new neuroprotectant which blocks N-methyl-D-aspartate responses. *J. Med. Chem*. **1995**, *38*, 3138-3145.

(19) Menniti F; Chenard B; Collins M; Ducat M; Shalaby I; White F. CP-101,606, a potent neuroprotectant selective for forebrain neurons. *Eur. J. Pharmacol.* **1997**, *331*, 117-126.

(20) Merchant, R. E.; Bullock, M. R.; Carmack, C. A.; Shah, A. K.; Wilner, K. D.; Ko, G.; Williams, S. A. A double-blind, placebo-controlled study of the safety, tolerability and pharmacokinetics of CP-101,606 in patients with a mild or moderate traumatic brain injury. *Ann N Y Acad Sci.* **1999**, *890*, 42-50.

(21) Liverton, N. J.; Claiborne, C. F.; Claremon, D. A.; McCauley, J. A. Heteroarylamino-Substituted 3-Fluoro-piperidines as NMDA/NR2B Antagonists, and their Preparation, Pharmaceutical Compositions, and Methods of Use. PCT Int. Appl. WO 2004108705 A1, 2004.

(22) Addy C.; Assaid C.; Hreniuk D.; Stroh M.; Xu Y.; Herring W. J.; Ellenbogen A.; Jinnah H. A.; Kirby L.; Leibowitz M. T.; Stew-art R. M.; Tarsy D.; Tetrud J.; Stoch S. A.; Gottesdiener K.; Wagner J. Single-dose administration of MK-0657, an NR2B-selective NMDA antagonist, does not result in clinically meaningful improvement in motor function in patients with moderate Parkinson's disease. *J. Clin. Pharmacol.* **2009**, 49, 856–864.

(23) Ibrahim, L.; DiazGranados, N.; Jolkovsky, L.; Brutsche, N.; Luckenbaugh, D. A., Herring, W. J., Potter, W. Z., Zarate, C. A. Jr. A randomized, placebo-controlled, crossover pilot trial of the oral selective NR2B antagonist MK-0657 in patients with treatment-resistant major depressive disorder. *J. Clin. Psycho-pharmacol.* **2012**, *32*, 551–557.

(24) Paterson, B.; Fraser, H.; Wang, C.; Marcus, R. A Random-ized, double-blind, placebo-controlled, sequential parallel study of CERC-301 in the adjunctive treatment of subjects with severe depression and recent active suicidal ideation despite antidepressant treatment. Presented at the 2015 National Network of Depression Centers Annual Conference, November 15, Ann Arbor, MI, USA.

(25) Cerecor. https://ir.cerecor.com/press-releases/detail/30/cerecor-reports-top-line-data-from-cerc-301-phase-2-study (accessed Jun 03, 2020).

(26) Wilkinson, S. T.; Sanacora, G. A new generation of antidepressants: an update on the pharmaceutical pipeline for novel and rapid-acting therapeutics in mood disorders

based on glutamate/GABA neurotransmitter systems. *Drug Discovery Today*. **2019**, *24*, 606-615.

(27) Schroeder, M. C.; Hamby, J. M.; Connolly, C. J. C.; Grohar, P. J.; Winters, R. T.; Barvian, M. R.; Moore, C. W.; Boushelle, S. L.; Crean, S. M.; Kraker, A. J.; Driscoll, D. L.; Vincent, P. W.; Elliott, W. L.;. Lu, G. H.; Batley, B. L.; Dahring, T. K.; Major, T. C.; Panek, R. L.; Doherty, A. M.; Showalter, H. D. H. Soluble 2-substituted aminopyrido[2,3-d]pyrimidin-7-yl ureas. Structure-activity relationships against selected tyrosine kinases and exploration of in vitro and in vivo anticancer activity. *J. Med. Chem.* **2001,** *44,* 1915-1926.

(28) Lipinski, C. A. Drug-like properties and the causes of poor solubility and poor permeability. *J. Pharmacol. Toxicol. Methods*, **2000**, *44*, 235-249.

(29) Chrovian, C. C.; Soyode-Johnson, A.; Wall, J. L.; Rech, J. C.; Schoellerman, J.; Lord, B.; Coe, K. J.; Carruthers, N. I.; Nguyen, L.; Jiang, X.; Koudriakova, T.; Balana, B.; Letavic, M. A. 1*H*-Pyrrolo[3,2-*b*]pyridine GluN2B-selective negative allosteric modulators. *ACS Med. Chem. Lett.* **2019**, *10*, 261-266.

(30) Dalmau, J.; Gleichman, A. J.; Hughes, E. G.; Rossi, J. E.; Peng, X.; Lai, M.; Dessain, S. K.; Rosenfeld, M. R.; Balice-Gordon, R.; Lynch, D. R. Anti-NMDA-receptor encephalitis: case series and analysis of the effects of antibodies. *Lancet Neurol.*, **2008**, *7*, 1091-1098.

(31) DeGiorgio, L. A.; Konstantinov, K. N.; Lee, S. C.; Hardin, J. A.; Volpe, B. T.; Diamond, B. A subset of lupus anti-DNA antibodies cross-reacts with the NR2 glutamate receptor in systemic lupus erythematosus. *Nat. Med.*, **2001**, *7*, 1189-1193.

(32) Tsai, G. E. Ultimate Translation: Developing Therapeutics Targeting on N-Methyl-D-Aspartate Receptor. In *Neuropsychopharmacology: A Tribute to Joseph T. Coyle;* Schwarcz, R., Coyle, J. T., Eds; Academic Press: Cambridge, 2016; 257-309.

(33) Bear, M. F. Bidirectional synaptic plasticity: from theory to reality. *Philos. Trans. R. Soc. Lond. B. Biol. Sci.* **2003**, *358*, 649–655.

(34) Dudek S. M.; Bear M. F. Homosynaptic long-term depression in area CA1 of hippocampus and effects of N-methyl-D-aspartate receptor blockade. *Proc. Natl. Acad. Sci.* **1992**, *89*, 4363-4367.

(35) Duman, R. S.; Aghajanian, G. K.; Sanacora, G.; Krystal, J. H. Synaptic plasticity and depression: New insights from stress and rapid-acting antidepressants. *Nat. Med.* **2016**, *22*, 238–249.

(36) Letavic, M. A; Savall, B. M.; Allison, B. B.; Aluisio, L.; Andres, J. I.; De Angelis, M.; Ao, H.; Beauchamp, D.; Bonaventure, P.; Bryant, S.; Carruthers, N. I., Ceusters M.; Coe, K.; Dvorak, C. A.; Fraser, I.; Gelin, C. F.; Koudriakova, T.; Liang, J.; Lord, B.; Lovenberg, T.; Otieno, M.; Schoetens, F.; Swanson, D.; Wang, X.; Wickenden, A.; Bhattacharya, A. 4-Methyl-6,7-dihydro-4*H*-triazolo[4,5-c]pyridine-based P2X7 receptor antagonists: optimization of pharmacokinetic properties leading to the identification of a clinical candidate. *J. Med. Chem.* **2017**, *60*, 4559-4572.

(37) Swanson, D. M.; Savall, B. M.; Coe, K. J.; Schoetens, F.; Koudriakova, T.; Skaptason, J.; Wall, J.; Rech, J.; Deng, X.; De Angelis, M.; Everson, A.; Lord, B.;Wang, Q.; Ao, H.; Scott, B.; Sepassi, K.; Lovenberg, T. W.; Carruthers, N. I.; Bhattacharya, A.; Letavic, M. A. Identification of (R)-(2-chloro-3-(trifluoromethyl)phenyl)(1-(5-fluoropyridin-2-yl)-4-methyl-6,7-dihydro-1H-imidazo[4,5-c]pyridin-5(4H)-yl)methanone (JNJ 54166060), a small molecule antagonist of the P2X7 receptor. *J. Med. Chem.* **2016**, *59,* 8535-8548.

(38) Chrovian, C. C.; Soyode-Johnson, A.; Peterson, A. A.; Gelin, C. F.; Deng, X.; Dvorak, C. A.; Carruthers, N. I.; Lord, B.; Fraser, I.; Aluisio, L.; Coe, K. J.; Scott, B.; Koudriakova, T.; Schoetens, F.; Sepassi, K.; Gallacher, D. J.; Bhattacharya, A.; Letavic, M. A. A dipolar cycloaddition reaction to access 6-methyl-4,5,6,7-tetrahydro-1*H*- [1,2,3]triazolo[4,5-*c*]pyridines enables the discovery synthesis and preclinical profiling of a P2X7 antagonist clinical candidate. *J. Med. Chem*. **2018**, *61*, 207−223.

For Table of Contents Only

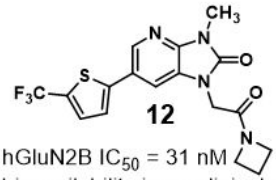

12

hGluN2B IC_{50} = 31 nM

bioavailability in preclinical species: 41-100%

rGluN2B receptor occupancy ED_{50} = 1.4 mg/kg

brain / plasma distribution (rat) = 1:1

good permeability; no PGP efflux / poor solubility

Human dose prediction from nanosuspension : 120 mg